USGS Award No. 07HQGR0152

USING REMOTE SENSING TO DOCUMENT LANDSLIDES FROM THE 2004 NIIGATA EARTHQUAKE

FINAL TECHNICAL REPORT

SUBMITTED: 10 July 2009

Ellen M. Rathje, Ph.D., P.E.
University of Texas at Austin
ECJ 9.227, C1792
Austin, TX 78712
Tel: 512-471-4929
Fax: 512-471-6548
e.rathje@mail.utexas.edu
http://www.caee.utexas.edu/dept/area/geotech/GeotechnicalEngr.htm

NEHRP Element: III
Key Words: Earthquake Effects, Landslides, Ground Failure

Research supported by the U.S. Geological Survey (USGS), Department of the Interior, under USGS award number (07HQGR0152). The views and conclusions contained in this document are those of the authors and should not be interpreted as necessarily representing the official policies, either expressed or implied, of the U.S. Government

ABSTRACT

Earthquake-induced landslides pose serious threats to lives and property across the world. These landslides typically occur in seismically active areas which exhibit steep topography, such as mountainous regions of Japan and China and the states of California, Oregon, Washington, and Utah within the United States.

Landslides caused by the 2004 Niigata-Ken Chuetsu earthquake in Japan were mapped using high resolution and lower resolution optical satellite imagery as a case study for developing semi-automated techniques to rapidly map earthquake-induced landslides. Post-event classification of high-resolution imagery was performed using (1) supervised pixel-based classification techniques, including the maximum likelihood, Bayesian pairwise, and Binary hierarchical methods, and (2) object-based classification techniques. The landslide inventories developed via satellite imagery were compared with a landslide inventory developed by traditional aerial survey. These comparisons indicated that the Bayesian hierarchal method produced the highest quality pixel-based classification, while the object-oriented classification produced higher-quality classifications than any of the pixel-based techniques. Change detection performed using pre- and post-event LANDSAT imagery provided a rapid and relatively accurate assessment of the landslide distribution across the affected area. However, the lower resolution caused the analysis to miss smaller landslides.

NON-TECHNICAL SUMMARY

Earthquake-induced landslides represent a significant earthquake hazard. Rapid assessments of landslide distribution after an earthquake can be obtained from satellite imagery. Additionally, these landslide distributions can be used in ongoing research efforts to improve our models that predict earthquake-induced landslides. This study investigated various techniques to develop landslide maps from satellite imagery. Satellite data from the 2004 Niigata-ken Chuetsu earthquake in Japan was used for the analyses. The results showed that earthquake-induced landslide distributions can be derived from satellite imagery, but that object-based and change detection approaches provide the most accurate results.

INTRODUCTION

Earthquake-induced landslides pose serious threats to lives and property across the world. These landslides typically occur in seismically active areas which exhibit steep topography, such as mountainous regions of Japan and China and the states of California, Oregon, Washington, and Utah within the United States. Earthquake-induced landslides pose serious threats in several ways. The direct impact of an earthquake-induced landslide can destroy and bury buildings and infrastructure. Secondary effects may also occur, such as blockage or destruction of vital transportation arteries and telecommunication lines. Secondary effects can be responsible for further losses of life due to the difficulties encountered by rescuers who must battle with blocked roadways and a lack of communication between affected areas.

Due to the severe threat posed by earthquake-induced landslides, research into this phenomenon is vital. For earthquake-induced landslides to be adequately researched after an event, their locations need to be identified so reconnaissance efforts can be adequately focused. Additionally, the developed landslide inventories can be used to validate and improve methodologies for predicting earthquake-induced landslides.

The study of earthquake-induced landslides typically involves the use of aerial photography, ground observations, and more recently, satellite imagery and GIS information. Landslide mapping using aerial photography was probably first used after the 1948 magnitude 7.3 Fukri, Japan earthquake (Keefer 2002). Before the advent of aerial photography, landslide mapping was limited to ground-based studies by teams of geologists and engineers. While ground-based studies are still an extremely important part of landslide mapping, this approach results in only limited observations because of access issues. Aerial photography, and now satellite imagery, allows an entire affected area to be examined, making the developed landslide inventories more complete.

The mapping of earthquake-induced landslides for research and response purposes occurs at several different scales. For immediate use by relief efforts, maps do not need to be exceptionally accurate, and only need to show which areas are most damaged and are in need of immediate attention. Maps are also useful for locating secondary threats such as landslide dams that create temporary lakes, which may breach and further threaten the lives of people downstream. Maps for this purpose are typically produced using manual interpretation of satellite imagery. Although manual interpretation may be fairly accurate, it can take many hours to days to interpret a single scene of satellite imagery or aerial photography. Human errors in interpretation may also occur. As a result, raw satellite imagery is often distributed to response personnel, without any prior manual interpretation performed.

Due to the amount of time needed to manually interpret satellite imagery and the potential for errors in manual interpretation, semi-automated image analysis offers an alternative for rapidly producing damage maps. Even if landslide and damage maps using this approach are produced too slowly for immediate response efforts, they can be used by reconnaissance teams visiting the area to study the damage.

The goal of this research is to investigate semi-automated techniques that use satellite imagery to generate maps of earthquake-induced landslides from the 2004 Niigata-Ken Chuetsu Earthquake in Japan ($M_w = 6.6$). A landslide inventory map is available from the Geographical Survey Institute (GSI) of Japan, which provides important ground truth data to which to compare the results from the analysis of the satellite imagery.

THE NIIGATA-KEN CHUETSU EARTHQUAKE IN JAPAN

The October 23, 2004 Niigata-Ken Chuetsu Earthquake (M_w=*6.6*) was the largest and most damaging earthquake to affect Japan after the 1995 Kobe earthquake. The epicenter was located in the Uonuma Hills, an upland region about 80 km south of Niigata City and 195 km northwest of Tokyo. The earthquake caused the deaths of 48 people, injured another 4,160, and temporarily displacement nearly 100,000 more. Several mountain villages were nearly completely destroyed, resulting in the permanent displacement of an unknown number of people (Scawthorn and Rathje 2006).

Cities affected by the earthquake include Nagaoka (population 194,000), Ojiya (population 41,000), Kawaguchi (population 5,748), and Yamakoshi (population 2,222). Many other small villages were also affected. Figure 1 shows the area affected by the earthquake. Damage was extensive to buildings and infrastructure across the area, with approximately 3,000 building collapses and an additional 100,000 buildings damaged. Approximately 1,000 buildings collapsed and 50,000 buildings were damaged in the town of Nagaoka alone. Roads and highways were damaged in over 6,000 locations, mainly due to ground failure and landslides. A Shinkansen (bullet) train, traveling at over 200 km/hr, was derailed by the earthquake. Other transportation structures, such as bridges, performed remarkably well, and no collapses occurred due to ground shaking (Scawthorn and Rathje 2006).

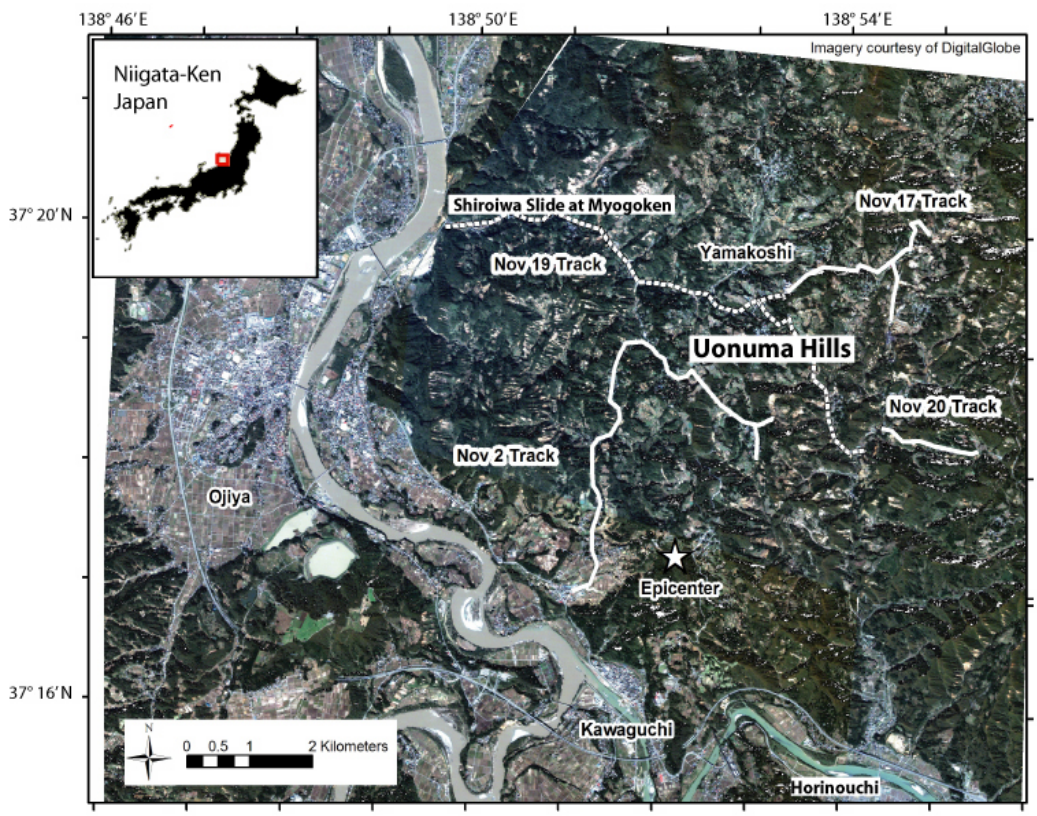

Figure 1. Location affected by the 2004 Niigata-ken Chuetsu earthquake in Japan (Rathje et al. 2006).

The earthquake occurred in a region of historically high seismicity. The epicenter of the earthquake is located 4 km east of Ojiya at 37.30° N, 138.84° E. Recorded ground motions include peak horizontal ground accelerations (PGA) as large as 1.75 g and peak horizontal ground velocities (PGV) as large as 53.1 cm/s (Scawthorn and Rathje 2006).

The most striking element of the Niigata-Ken Chuetsu earthquake is the number and extent of landslides caused by the event. Landslides occurred across an area of approximately 250 km^2, with the densest landslides occurring in an area of roughly 100 km^2 around the epicenter. The Niigata Prefecture (local government) officially documented 442 landslides caused by the earthquake; however researchers visiting the field noted that more had likely occurred, possibly up to 1,000 in number (Scawthorn and Rathje, 2006). Monetary damages caused by the landslides were estimated at U.S. $8 billion (Kieffer et al. 2006).

The geology of the area is characterized by weak and folded sedimentary rocks (Kieffer et. al. 2006). In addition to the relatively unstable geology, a record-setting typhoon season in the months preceding the earthquake elevated groundwater levels across the region, with Nagaoka recording 100 mm of rainfall on October 20 and another 13 mm on October 21. Elevated groundwater levels likely contributed to the large number of landslides due to higher than normal pore pressures (Scawthorn and Rathje 2006).

Landslides across the area consisted of many different sizes and types, including translational soil slides, deep-seated rotational slumps, debris flows, large block slides in bedrock, and many slides that were combinations of several different types. Landslide concentrations were found to be very high in some areas, with up to 35% of the ground surface over a single square kilometer being covered by landslides (Kieffer et al. 2006). Landslide concentrations were found to be remarkably similar to the 1994 Northridge earthquake in California, although soil moisture was very low when the Northridge earthquake occurred, compared to highly saturated soils during the Niigata-Ken Chuetsu earthquake (Kieffer et al. 2006).

AVAILABLE SATELLITE IMAGERY

Satellite imagery available for the 2004 Niigata earthquake includes high-resolution Quickbird and IKONOS scenes collected after the earthquake and lower-resolution LANDSAT scenes collected before and after the earthquake (Table 1). Although data from the Quickbird satellite has the highest spatial resolution of any data available for this event (2.4 m multispectral, 0.6 m panchromatic), the imagery was collected at a very poor acquisition angle of 47° (0° indicates pure vertical acquisition), which resulted in a large amount of distortion in the imagery. The IKONOS data was also collected at a better, but still poor, acquisition angle (36°), and the data appears less distorted than the Quickbird data. Because of the poor imagery from the Quickbird sensor, analyses performed using the Quickbird data are not presented in this report. Pre-event high resolution satellite imagery was also available for the affected area, but because of the poor acquisition angles of the post-earthquake imagery it could not be co-registered with the pre-event imagery and for change detection analysis.

The IKONOS imagery of the affected area is shown in Figure 2. Only the multispectral bands were used for analysis, due to their higher spectral resolutions. The panchromatic band contains wavelengths within the bounds of the visible light and near-infrared bands, and thus adds little new spectral information, although the spatial resolution is higher.

Data collected from the LANDSAT 7 ETM+ sensor was used to perform a change detection analysis over the affected area. Pre- and post-event imagery were collected on July 5, 2004 and November 10, 2004, respectively. These dates were selected because data acquired on dates closer to the earthquake were badly cloud covered. The area affected by the earthquake is included within a single LANDSAT scene, and the imagery exhibited no cloud cover over the area of interest in the pre-event data and very little could cover in the post-event data. The LANDSAT data is shown in Figure 3.

Table 1. Satellite imagery used in this study

Data Type	Spatial Resolution	Collection Date
Quickbird Multispectral Imagery	2.4 m multispectral 0.6 m panchromatic	October 24, 2004
IKONOS Multispectral Imagery	4.0 m multispectral 1.0 m panchromatic	October 24, 2004
LANDSAT 7 ETM+ Multispectral Imagery	30 m multispectral 15 m panchromatic	July 5, 2004 November 10, 2004

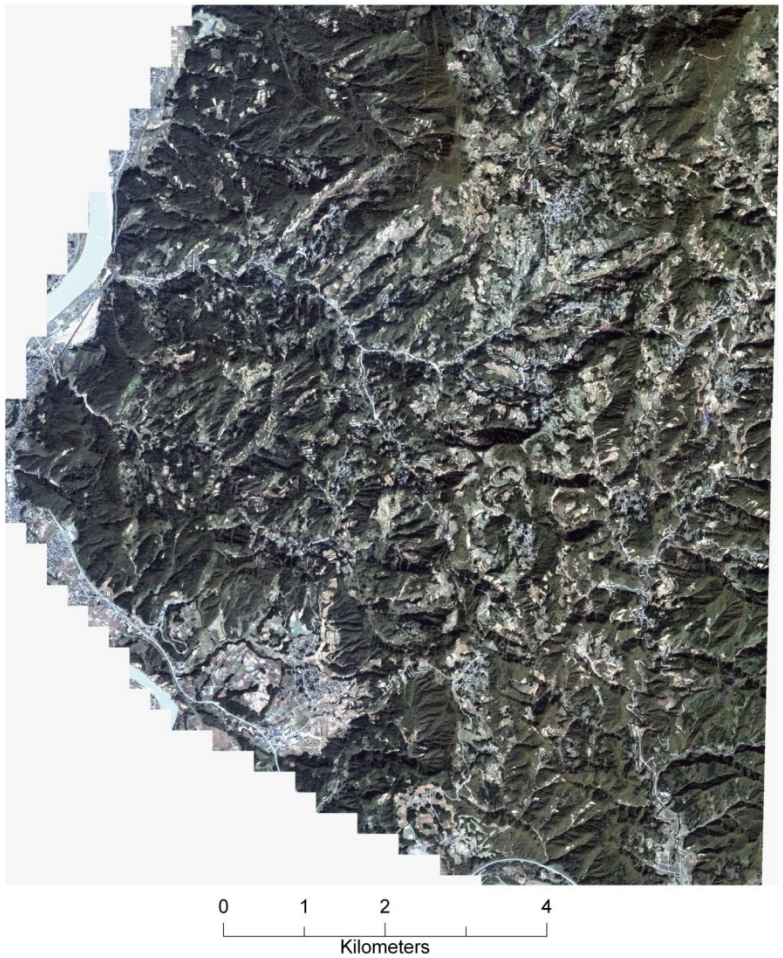

Figure 2. IKONOS imagery for Niigata-Ken Chuetsu Earthquake, displayed in true-color format

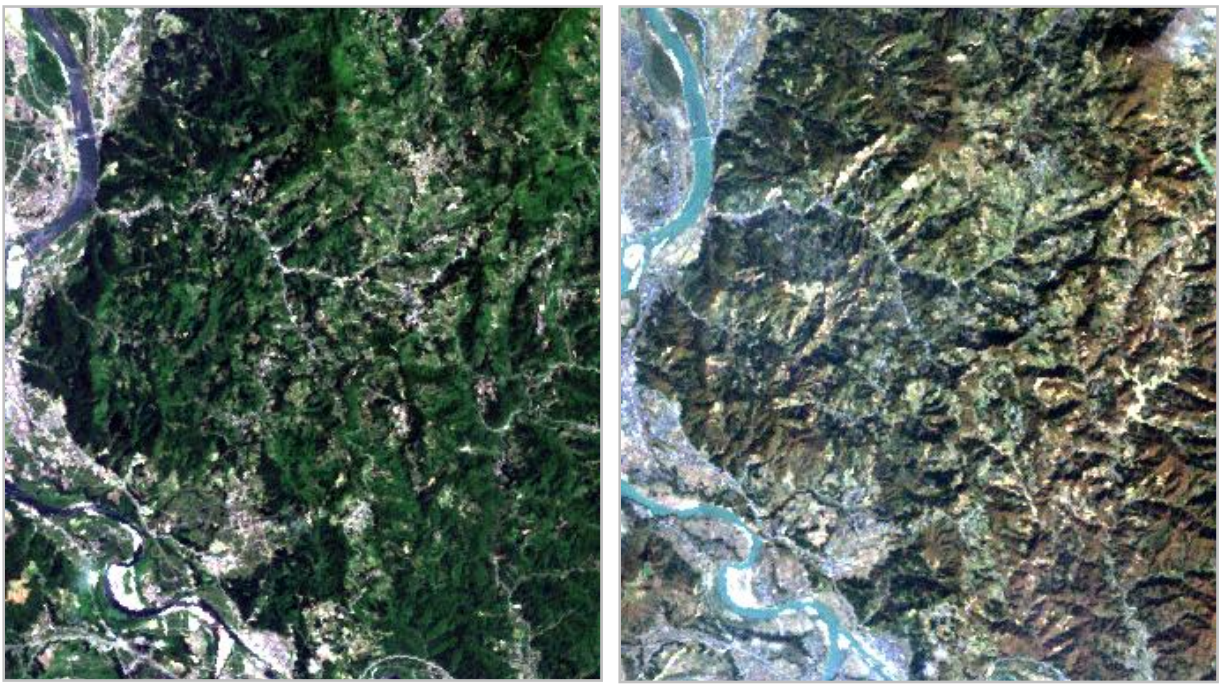

(a) (b)

Figure 3. (a) Pre-event and (b) post-event LANDSAT imagery for the Niigata-ken Chuetsu earthquake

PIXEL-BASED CLASSIFICATION OF HIGH-RESOLUTION IMAGERY

Land Cover Classes and Training Data

One of the most important aspects of image classification is the definition of a set of land cover classes. For landslide identification the only land cover of interest is landslides and related features, and an accurate classification of other land covers is not needed. However, to properly perform a pixel-based classification, appropriate land cover classes must be selected so that all major types of land cover in the imagery are accurately separated from the class of interest (i.e., landslides).

The area over which imagery was collected can generally be described as a patchwork of forest, small villages, and agricultural areas consisting of rice paddies and ponds for the production of ornamental koi fish, many of which are terraced into the upland areas (Figure 2). Forested land, dissected by roads linking villages, occupies the majority of the upland areas. Surrounding the upland area are the alluvial plains of the Shinano and Uono rivers, which are mostly covered in rice paddies and other agricultural areas. Earthquake induced landslides are readily visible across the upland areas of the landscape. The landslides stripped away large amounts of vegetation and soil, depositing the subsequent debris in flatter areas adjacent to the source zones. Additional effects of the landslides include muddy water, formed by sediment-laden runoff. Shadows are also common in the imagery, with many areas returning low reflectance values due to being shaded by slopes.

A set of classes was designated by visual inspection of the imagery and trial classifications. The final hierarchy includes eight classes:

1. landslides
2. landslide debris
3. muddy water
4. agricultural
5. water
6. urban
7. vegetation
8. shadows

These classes were found to cover all of the commonly occurring land visible in the imagery, and they include the two land covers of primary interest: landslides and landslide debris. The landslides class is defined as brightly colored regions corresponding to areas of stripped vegetation and exposure of soil and bedrock on steep hillsides, and represents the majority of landslides visible in the imagery. The landslide debris class represents darker colored areas associated with landslide. This class represents both debris deposited by landslides (mixtures of soil, rock, vegetation, and other debris) and some landslides that are darker than the landsides represented by the landslide class. The landslide debris class is typically found downslope from or adjacent to brightly colored landslides, although some landslides may appear more as landslide debris in their entirety. The landslides and landslide debris classes are not combined initially due to large amounts of spectral overlap between the landslide debris class and the agricultural class, resulting in confusion. The landslides class is much more spectrally unique from the other classes in the imagery, so confusion with other classes is less of a problem. Figure 4 shows a small area of imagery with selected areas of each class overlain.

To provide the most objective comparison between each pixel-based classifier, a common set of training data was selected for use with each method. Training data collection consisted of selecting small groups of pixels representative of each class across the imagery. Care was taken not to select edge pixels, or pixels in the transition zone between different classes. A consistent number of pixels of training data, between 1000 and 1100, were selected for each class, corresponding to a total area on the ground of 16,000 to 18,000 m^2 in size. This amount of data was selected to provide an adequate amount of information to produce representative histograms and class probability estimates. Selection of additional training data is very time consuming and was not found to increase the accuracy of the classification. Each individual area of training data was typically 40-60 pixels in size.

Features represent the characteristic of each pixel used in the classification. Features used for classification consisted of the four multispectral bands from the IKONOS sensor, including the blue (wavelength 445 – 516 nm), green (506 – 595 nm), red (632 – 698 nm), and near-infrared (757 – 853 nm) bands.

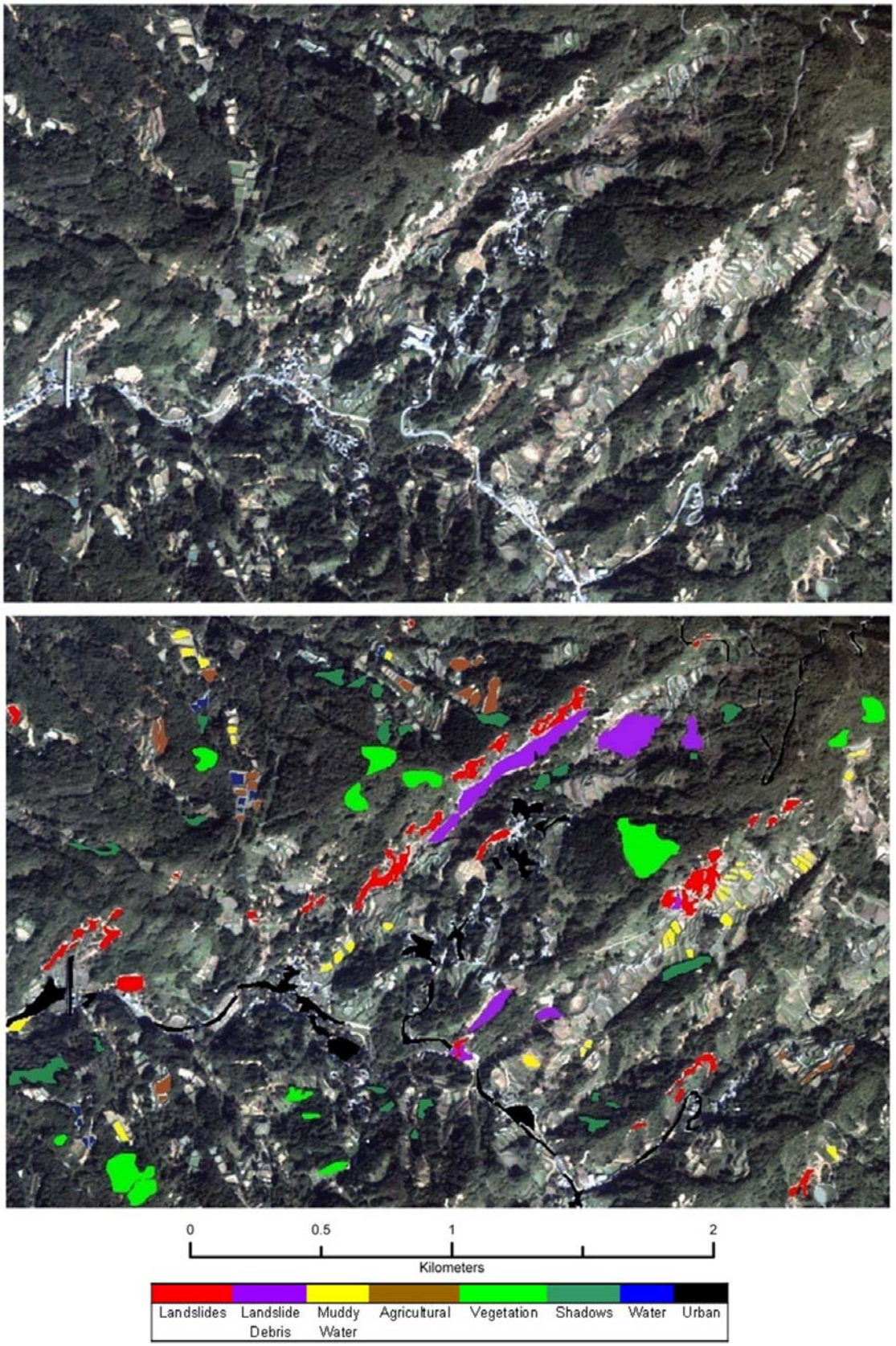

Figure 4. Land cover classes for pixel-based classification

Accuracy Assessment

Each pixel-based classification technique was used to analyze the post-earthquake imagery and place each pixel into one of the eight land cover classes. Accuracy, which can be defined both quantitatively and qualitatively, is one the most important aspects of any classification. Quantitative accuracy assessments compare the classified product to *ground truth*, or accurate knowledge of which classes are present at selected locations on the ground. Ground truth can be collected in several ways, with the most robust data obtained by visiting the field and performing a survey, noting land cover and geographic coordinates at a number of locations across the imagery. This approach is not always possible due to time and budgetary constraints. Alternatively, ground truth can be manually selected directly from the remotely-sensed data itself, as long as care is taken to select ground truth data that does not include areas selected as training data. This method of ground truth selection is less desirable than an actual field visit, as user errors during selection may occur; however it is far cheaper and easier to perform.

Comparison between classified imagery and ground truth can be performed in several different ways. *Non-site-specific accuracy* represents a comparison of the total areas for each class in the ground truth and the classified image over the same spatial area. Non-site-specific accuracy assessments are useful in situations where ground truth is available separately from the imagery, such as a map of land cover in the area produced by another study, or where the ground truth and classified imagery cannot accurately be georeferenced to one another (Campbell 2007). Non-site-specific accuracies may be overly conservative or liberal in their assessments of accuracy. For example, a classification may return 1.5 km^2 of a class and the ground truth may show 1.6 km^2 of the same class, indicating a high accuracy for the classification. However, these areas may not spatially overlap in all areas, and the true accuracy of the classification may be less than computed by the non-site-specific accuracy. As a result, non-site-specific accuracies can sometimes mask large classification errors (Campbell 2007).

Site-specific accuracies offer a more detailed accuracy assessment by taking into account the classification of individual pixels or objects relative to their ground truth classification. High-precision location information is required for ground truth data to perform a proper site-specific accuracy assessment. Small errors between the actual and recorded locations of ground truth can lead to erroneous classification accuracies. Either ground truth data collection using a site survey with detailed GPS locations or accurate collection of ground truth from the same imagery used in the classification is required (Campbell 2007).

For this study, the accuracy of the classified images was assessed using three methods: site-specific accuracy based on visually identified ground truth from the imagery (but not including pixels used in training), non-site-specific accuracy in the form of a landslide density comparison using the GSI landslide map, and a qualitative accuracy based on visual comparison of the classification and GSI map. Ground truth for the site-specific accuracy assessment was selected in much the same way as training data. Small groups of pixels, typically 50 to 150 pixels in size, were selected across the imagery, with a total of between 2,000 and 2,025 pixels of ground truth selected for each class.

Maximum-Likelihood Classification

Maximum-likelihood classification (MLC) involves developing probability density functions for each class using the training data, and then assigning each pixel to the class to which it has the highest probability of being a part. The maximum likelihood classification was performed using the image analysis software, ENVI 4.3 (ITT Industries, Inc).

Examination of the classified image revealed that many small incorrectly classified groups of pixels were present, typically on the order of 1-5 pixels in size. To remove these small, incorrectly classified pixel groups, post-processing in the form of a majority analysis was performed. A majority analysis uses a two-dimensional matrix centered on every pixel, and assigns the pixel in the center to the class which occurs most throughout the rest of the matrix. A 3x3 matrix was used here so that the classification details were maintained. Larger matrices produced a smoother appearance, but remove much of the original classification detail.

The *site specific accuracy* was evaluated through a confusion matrix that compares the classes of the ground truth pixels to the classes assigned by the classification analysis. The confusion matrix for the MLC classification is shown in Table 2, and indicates an overall accuracy of nearly 87%. However, there is considerable confusion between the following class pairs: landsides and landslide debris; landslide debris and agricultural; and landslides and muddy water. Confusion between the landslide and landslide debris classes are not surprising, and they are not of concern because these classes will be combined to develop the landslide inventory. Confusion is the largest between the agricultural and landslide debris classes, as nearly 25% of the pixels identified as agricultural in the ground truth data were classified as landslide debris by the analysis. This commission error within the landslide debris class is potentially problematic because it may lead to overestimation of landslide inventory.

Table 2. Confusion matrix for the MLC classification

	Ground Truth									
Classification	*Landslides*	*Landslide Debris*	*Agricultural*	*Muddy Water*	*Vegetation*	*Water*	*Shadows*	*Urban*	*Commission Error*	*Omission Error*
Landslides	78.1	2.6	0.0	11.2	0.0	0.0	0.0	0.0	15.0	21.9
Landslide Debris	14.2	74.9	24.9	7.8	0.2	0.2	0.1	0.4	38.7	25.1
Agricultural	0.2	16.8	75.0	0.4	0.0	0.7	0.0	1.4	20.7	25.1
Muddy Water	7.0	3.4	0.0	74.8	0.0	0.0	0.0	0.0	12.2	25.2
Vegetation	0.5	1.4	0.1	0.0	99.8	0.1	2.7	0.4	4.9	0.2
Water	0.0	0.1	0.0	0.0	0.0	96.0	0.0	0.0	0.1	4.0
Shadows	0.0	0.0	0.0	0.0	0.0	0.0	96.3	0.0	0.0	3.7
Urban	0.1	0.9	0.2	5.8	0.0	3.1	1.0	97.9	10.2	2.1
Total Accuracy	86.6	*Kappa Coefficient*			0.85					

Non-site-specific accuracy was evaluated by comparing landslide densities obtained from the MLC classification to those from the GSI landslide map. This analysis was performed by georeferencing the landslide map to the IKONOS data and dividing up both the classified image and the uplands region of the landslide map into 85, 1-km^2 blocks. The landslide density for each map block was computed for the GSI map by taking the total area of landslides in the block, defined by all mapped landslides and headscarps, and dividing by the total area (1 km^2) of the block. Landslide density for each classification block was computed by summing the total area

of both the landsides and landslide debris classes and dividing by the total area (1 km^2) of each block.

Landslide densities from the MLC classification (classified) are plotted versus the landslide densities from the GSI map (mapped) in Figure 5. While most of the plotted data does not lie on a 1:1 line, 74.1% of the blocks exhibit classified and mapped landslide densities within +/- 5 percentage points of one another. The data in Figure 5 show that at mapped landslide densities less than about 3%, the classification tends to overestimate landslide density. At mapped landslide densities larger 16% the MLC classification tends to underestimate landslide densities. The overestimation of landslide density by the MLC at small mapped landslide densities appears to be caused by overestimation of the landslides debris class, mainly due to commission errors with the agricultural class. The underestimation of landslide density by the MLC at larger mapped landslide densities appears to be caused by many landslides being covered by intact vegetation. Because the classification relies on stripped vegetation to indentify landslides, it will not accurately identify landslides that remain intact with overlying vegetation.

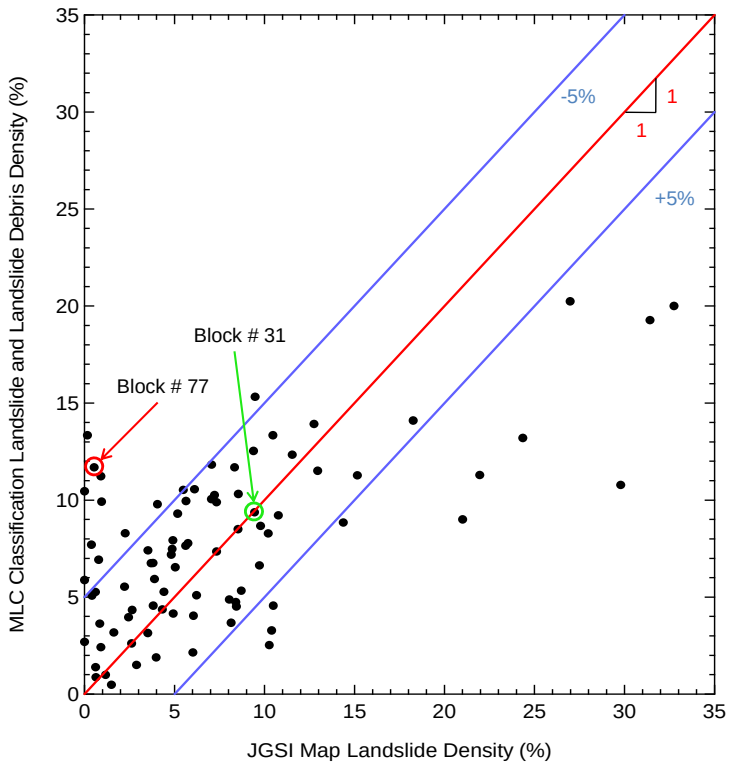

Figure 5. Landslide density comparison for MLC classification.

The *qualitative accuracy* of the MLC classification was determined by visually examining the classified image relative to the original multispectral data and GSI map. Generally the classification tended to greatly overestimate the area of landslide debris, mainly due to confusion with the agricultural class. The confusion matrix (Table 2) shows that the problem exists, but that it is relatively mild. Visual examination of the imagery indicates that the total area classified as landside debris is many times greater than the actual area of landslide debris. Other than the mass overestimation of landslide debris area, the classification appears to perform adequately, and captures most landslides that appear as the brightly colored areas of stripped vegetation and bare soil and/or rock.

Figure 6 shows a relatively typical subset of the MLC classification. The classification captures most of the landslides in the scene, but greatly overestimates the area of landslide debris. Again, this is due to the large amount of confusion and commission error between the landslide debris and agricultural classes. All other classes seem to be well-defined by the classification with relatively few classification errors.

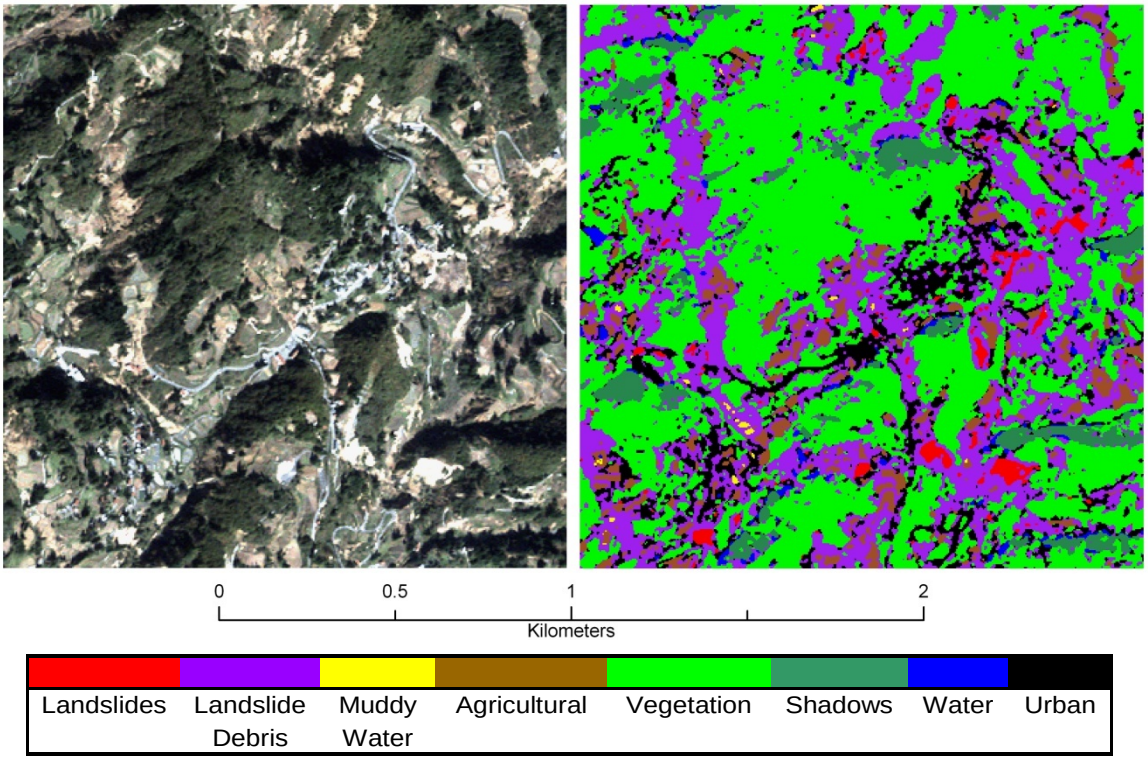

Figure 6. True-color IKONOS imagery and MLC classification over same spatial area

Bayesian Pairwise Classification

Bayesian Pairwise Classification (BPC) is an advanced classification technique that decomposes the classification problem containing C classes into $\binom{C}{2}$ two-class problems. For example, in a classification of landslides, forests, and urban, the BPC would perform separate classifications for each pixel for the following two-class problems: landslides vs. forests, landslides vs. urban, and forests vs. urban. The final classification of a pixel is performed by voting, where the classification results of each of the two-class problems are tallied and the pixel is assigned to the class to which it was classified the most often. Alternatively, the maximum posterior probability can be used to obtain the final classification (Crawford et al. 1999, Kumar et al. 1999). In addition to pairwise classification, the BPC includes a pairwise feature selection algorithm in which the most discriminating features are used for each class pair. The BPC classification procedure is implemented in the MATLAB-based Center for Space Research Classification Program (CSR-C). The BPC analysis was performed using the same training data, features, and spatial area as the MLC classification. A majority analysis using a 3x3 matrix was also performed on the BPC classification, to remove small incorrectly classified groups of pixels across the imagery.

The *site specific accuracy* of the BPC results was evaluated through a confusion matrix (Table 3). The confusion matrix indicates a high overall accuracy of 87.8%. These values are only slightly higher than for the MLC (Table 2). Further examination shows the greatest amount of confusion is between the landslide debris and agricultural classes, with confusion also occurring between the landslides class and both the muddy water and landslide debris classes. The confusion values are very similar to those from the MLC (Table 3). The classification error between the landslide debris and agricultural classes is large; with 21.6% of the ground truth for the agricultural class incorrectly classified as landslide debris. This confusion is reflected in a high commission error for the landslide debris class (~35%). The classification problem appears to be mainly in the overestimation of the landslide debris class area, as only 10.6% of the ground truth for the landslide debris class was incorrectly classified as agricultural.

Table 3. Confusion matrix for the BPC classification

	Ground Truth									
Classification	*Landslides*	*Landslide Debris*	*Agricultural*	*Muddy Water*	*Vegetation*	*Water*	*Shadows*	*Urban*	*Commission Error*	*Omission Error*
Landslides	78.9	2.9	0.0	11.7	0.0	0.0	0.0	0.1	15.7	21.2
Landslide Debris	15.3	82.2	21.6	6.3	0.0	0.2	0.1	0.7	34.8	17.8
Agricultural	0.2	10.6	77.7	0.2	0.1	0.6	0.0	1.0	14.1	22.3
Muddy Water	5.2	1.5	0.0	75.4	0.0	0.0	0.0	0.0	8.2	24.6
Vegetation	0.5	1.0	0.0	0.0	99.9	0.1	3.7	0.6	5.6	0.2
Water	0.0	0.0	0.0	0.0	0.0	94.7	0.0	0.0	0.0	5.3
Shadows	0.0	0.0	0.0	0.0	0.0	0.0	95.9	0.0	0.0	4.1
Urban	0.0	1.7	0.7	6.4	0.0	4.5	0.4	97.7	12.2	2.3
Total Accuracy	87.8	*Kappa Coefficient*			0.86					

Non-site-specific accuracy was evaluated by comparing the landslide densities obtained from the BPC classification and the landslide densities obtained from the GSI landslide map (Figure 7). Approximately 74% of the blocks exhibited classified and mapped landslide densities within +/- 5 percentage points of each other. This result is exactly the same as the MLC, and in fact, most of the BPC landslide densities are very similar to the MLC values. The BPC classification tends to overestimate landslide densities at small values of mapped landslide densities, typically less than 2%. These large discrepancies are caused by commission errors within the landslide debris class resulting from confusion with the agricultural class. At landslide densities greater than about 15%, the classification tends to underestimate landslide area due to some landslides being covered by vegetation. For mapped landslide densities between 2 and 15%, the BPC classification and the GSI landslide map are generally within 5 percentage points of each other.

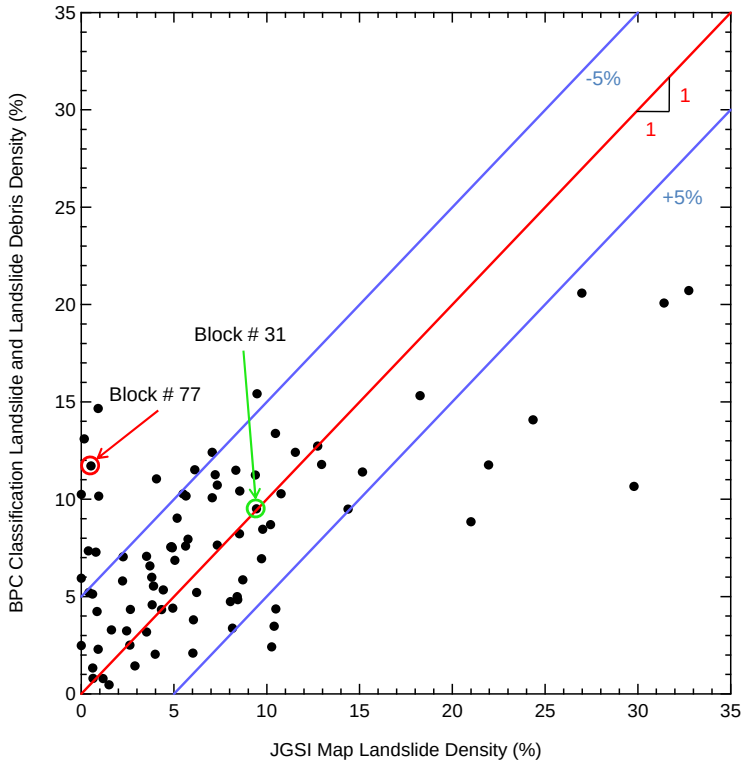

Figure 7. Landslide density comparison for the BPC classification.

The *qualitative accuracy* of the BPC classification was evaluated by visually examining the classified product relative to the original true-color multispectral imagery and GSI map. Similar to the MLC results, the BPC classification adequately identified most landslides that appear as bright areas of bare rock and soil. However, large amounts of overestimation of the landslide debris class were found across the image due to confusion with agricultural areas. Some commission errors in the urban class were also noticed where landslide debris and agricultural areas were incorrectly classified as urban. Figure 8 shows a representative area of the imagery classified using the BPC and it is the same area shown in Figure 6 for the MLC. Overestimation of the landslide debris area can be seen across the imagery, generally due to confusion with the agricultural class. However, the BPC identified more agricultural area than the MLC (Figure 6) making it somewhat more accurate.

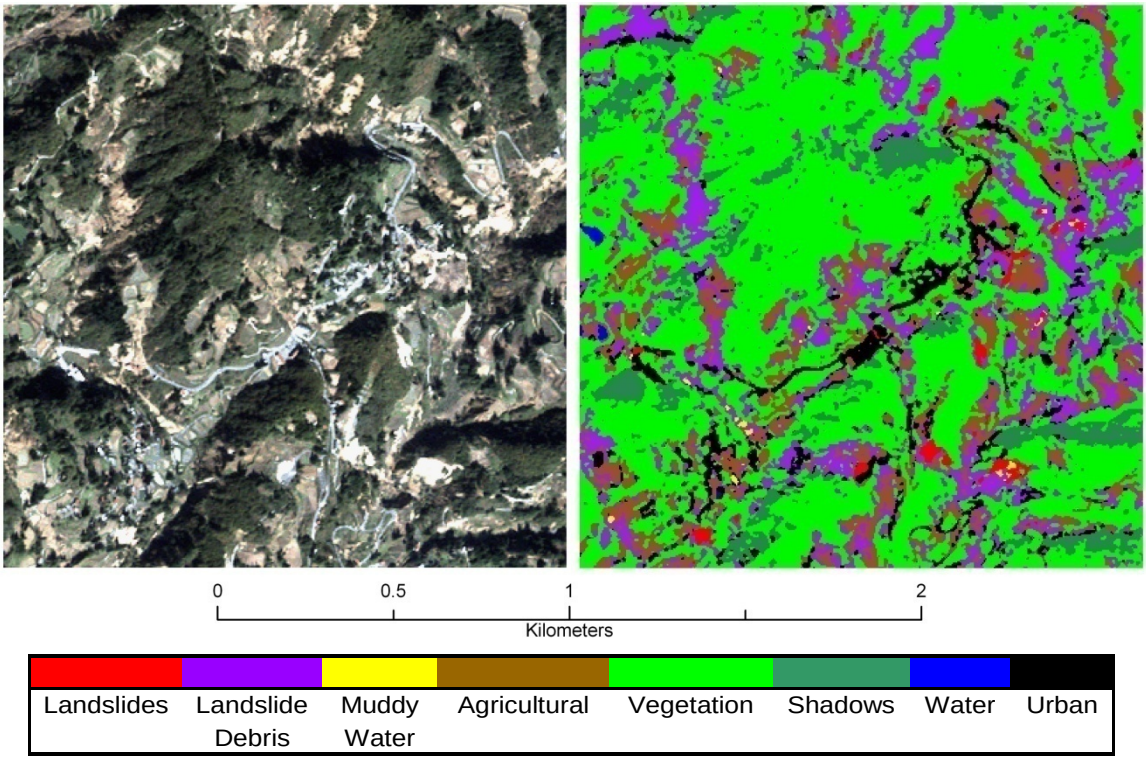

Figure 8. True-color IKONOS imagery and BPC classification over same spatial area.

Binary Hierarchical Classification

Binary Hierarchical Classification (BHC) is an advanced classification technique that divides a problem with *C* classes into a problem consisting of (*C-1*) two-class problems. The BHC automatically generates a class hierarchy using a top-down approach, where all classes are first lumped together and then split into smaller and smaller subclass groups until the desired classes are obtained. The BHC produces a decision tree consisting of *C* leaf nodes, each representing the original classes, and *C-1* internal nodes, where feature extraction and classification are performed (Kumar et al. 2002). The BHC classification procedure is also implemented in the MATLAB-based Center for Space Research Classification Program (CSR-C). The BHC analysis was performed using the same training data, features, and spatial area as the other classification techniques. A majority analysis using a 3x3 matrix was also performed on the classified product.

The *site specific accuracy* of the BPC results was evaluated through a confusion matrix (Table 4). The confusion matrix indicates a total accuracy of 83.1%, which is slightly smaller than the MLC and BPC. Considerable confusion exists between landslide debris and agricultural, landslides and landslide debris, and muddy water and landslides class pairs. The largest amount of confusion is between the landslide debris and agricultural classes. Both commission and omission errors are high for the landside debris class, at nearly 48 and 45%, respectively. These values are about 15 and 25% larger than for the MLC and BPC classifications. The largest problem appears to be a gross overestimation of the landslide debris class, resulting from confusion with the agricultural class. This is reflected by the high commission error. Omission errors are also fairly large for the landslide debris class, meaning fairly large amounts of landslide debris were incorrectly classified as agricultural.

Table 4. Confusion matrix, BHC classification

Classification	Ground Truth									
	Landslides	*Landslide Debris*	*Agricultural*	*Muddy Water*	*Vegetation*	*Water*	*Shadows*	*Urban*	*Commission Error*	*Omission Error*
Landslides	81.3	2.9	0.0	5.6	0.0	0.0	0.0	2.1	11.6	18.7
Landslide Debris	11.3	55.1	32.0	5.1	0.0	0.0	0.0	2.3	47.7	44.9
Agricultural	2.1	27.2	65.9	7.7	0.0	0.3	0.0	5.6	39.6	34.1
Muddy Water	4.5	4.1	0.0	81.0	0.0	0.0	0.0	0.1	9.7	19.0
Vegetation	0.7	5.5	0.1	0.0	100	0.0	4.19	1.9	11.1	0.0
Water	0.0	2.3	2.1	0.5	0.0	99.7	0.0	1.8	6.2	0.3
Shadows	0.0	0.1	0.0	0.0	0.0	0.0	95.7	0.0	0.1	4.3
Urban	0.1	2.8	0.0	0.1	0.0	0.0	0.2	86.1	3.5	13.8
Total Accuracy	83.1	*Kappa Coefficient*			0.81					

Non-site-specific accuracy was assessed by comparing classified and mapped landslide densities in the same manner as for the BPC and MLC classifications (Figure 9). The data in Figure 9 shows that 72.8% of the blocks exhibit classified landslide densities within +/- 5% of the mapped values. While this value is similar to that obtained for the MLC and BPC methods, the data in Figure 9 shows a more systematic underestimation of landslide density. The BHC classification tends to underestimate landslide density in many cases where the mapped landslide density exceeds about 8% and in all cases where the mapped density exceeds 13%. Overall, the landslide density plot indicates that the BHC tends to underestimate landslide density when compared to the mapped landslide density. This does not necessarily indicate poor performance, as the mapped landslide extents may be partially covered by vegetation or other land covers, which would not be classified as landslides.

The *qualitative accuracy* of the BHC classification was assessed by visually comparing the classified imagery with the multispectral data. It was found that, in general, the BHC accurately identified landslides appearing as brightly-colored areas of bare soil and rock, and confusion between the landslides class and other classes was relatively low. Additionally, there was relatively little overestimation of landslide debris area due to confusion between with the agricultural class, when compared to the MLC and BPC classifications. One interesting feature to note is that many commission errors were present in the water class, with some agricultural areas and even landslide debris being classified as water. However, the area of landslide debris misclassified as water is very low. Figure 10 shows representative area of the imagery classified using the BHC and it is the same area shown in Figures 6 and 8 for the other pixel-based classifications. The BHC accurately identifies all landslides in the imagery as landslides, and the overestimation of landslide debris is relatively low. Thus, while the confusion matrix indicated that the BHC classification had the same accuracy as the MLC and BPC, the qualitative assessment indicates that the BHC was superior.

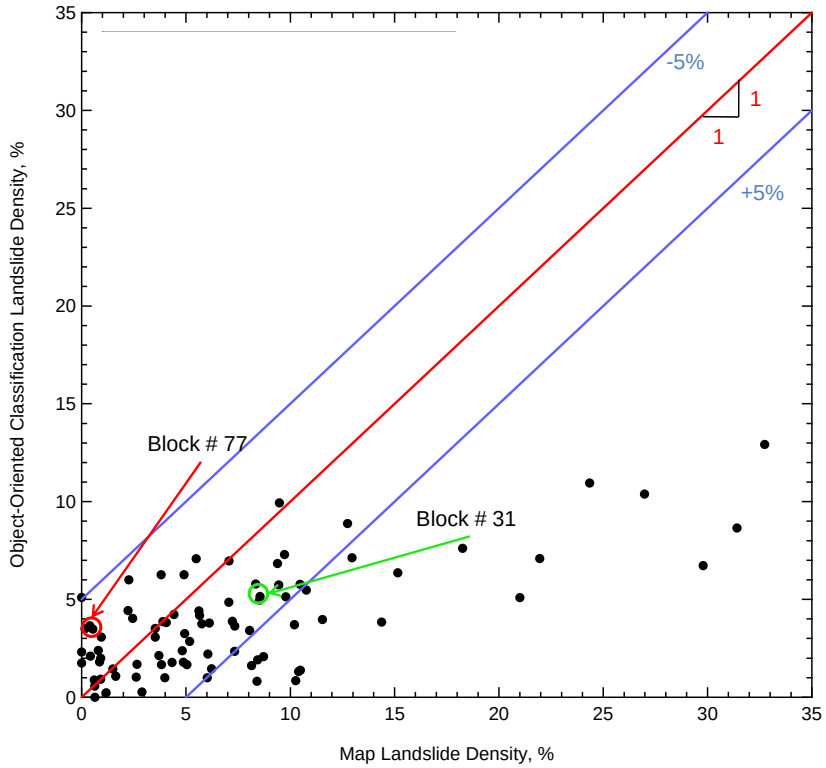

Figure 9. Landslide density comparison for BHC classification.

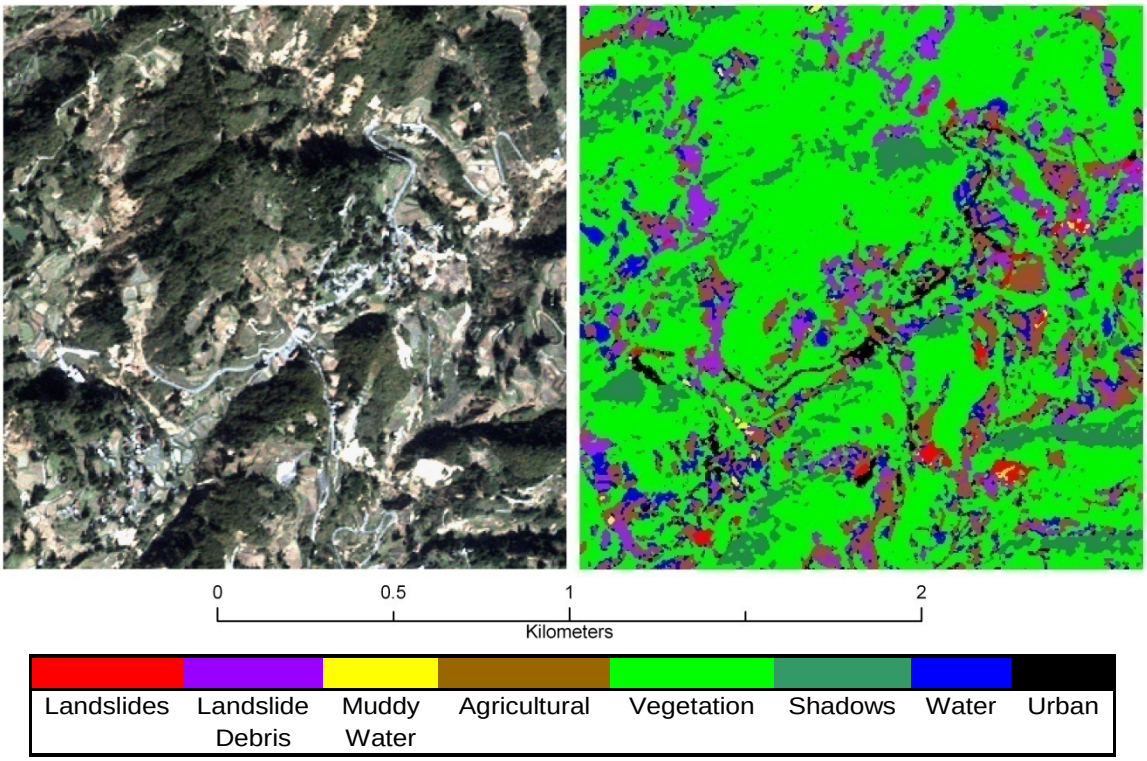

Figure 10. True-color IKONOS imagery and BHC classification over same spatial area.

OBJECT-BASED CLASSIFICATION OF HIGH-RESOLUTION IMAGERY

Object-oriented classification, performed using Definiens Developer 7.0 software from Definiens AG, offers the ability to overcome many of the weaknesses common with pixel-based classification methods. Object-oriented classification methods classify image objects rather than individual pixels, and can be performed on objects of varying size and shape. Object-oriented classifications can also utilize GIS-like post-classification procedures and rules, which can result in a final classified product optimized for the highest overall accuracy. The object-oriented classification performed for this research utilized the same multispectral IKONOS imagery as the pixel-based classifications.

Segmentation and Classification Procedures

The object-oriented classification utilizes only four final classes: landslides, landslide debris, vegetation/shadows, and "other". The landslides and landslide debris classes consist of similar land cover as the same classes used for the pixel-based classification, with the landslides class corresponding to brightly-colored areas of bare soil and rock, and the landslide debris class corresponding to darker areas of soil, rocks, trees, and other debris. The vegetation and shadows class contains all types of vegetation (trees, shrubs, grasses, etc) and shadows, and the "other" class contains all land covers that do not fall into the previously defined classes (i.e. other represents water, agricultural, urban, other, etc). As the goal of this classification is to identify only landslides and related features such as landslide debris, there is no need to further separate between classes of non-interest such as agricultural and urban. This approach also allows the sample selection process to be simplified, as samples for only four classes are required. This class hierarchy is considerably simpler than the eight class hierarchy used for the pixel-based classifications. The four-class hierarchy was selected due to the framework of the nearest-neighbor classifier, as opposed to the statistical classifiers used in the pixel-based classifications. As a result, classes can be constructed occurring over a wide range of land covers and spectral responses, provided that training samples are selected such that all representative spectral responses of each class are captured. The nearest-neighbor classifier does not model probability density functions, and therefore the histograms of each class can have any shape and an accurate classification can be performed, provided that proper sample selection is performed.

Segmentation is the first step in the object-oriented classification process. The goals of segmentation for this classification were to produce image objects of small size and homogeneous spectral properties that best represent the various types of land cover. To meet these goals, segmentation was performed using the four multispectral IKONOS bands, each set with an equal weighting of 1. The shape and compactness parameters were both equally set at 0.1, which resulted in image objects exhibiting homogeneous spectral properties and uneven shapes. The scale parameter was set at 1, which produced relatively small-sized image objects. Figure 11 shows a portion of the imagery before and after segmentation, and shows that the image objects tend to exhibit a size where individual rice paddies, ponds, and small landslides are each represented by a single image object.

Two nearest-neighbor classifications, a primary and a secondary, were performed (Figure 12). This process was selected to simplify the final classification between landslides and all other land cover types. The primary classification was performed to separate the vegetation/shadows class from all remaining land cover, and this internal class was named "non-vegetation/shadows". All nearest neighbor classifications were performed using the mean value of the IKONOS multispectral data within an object.

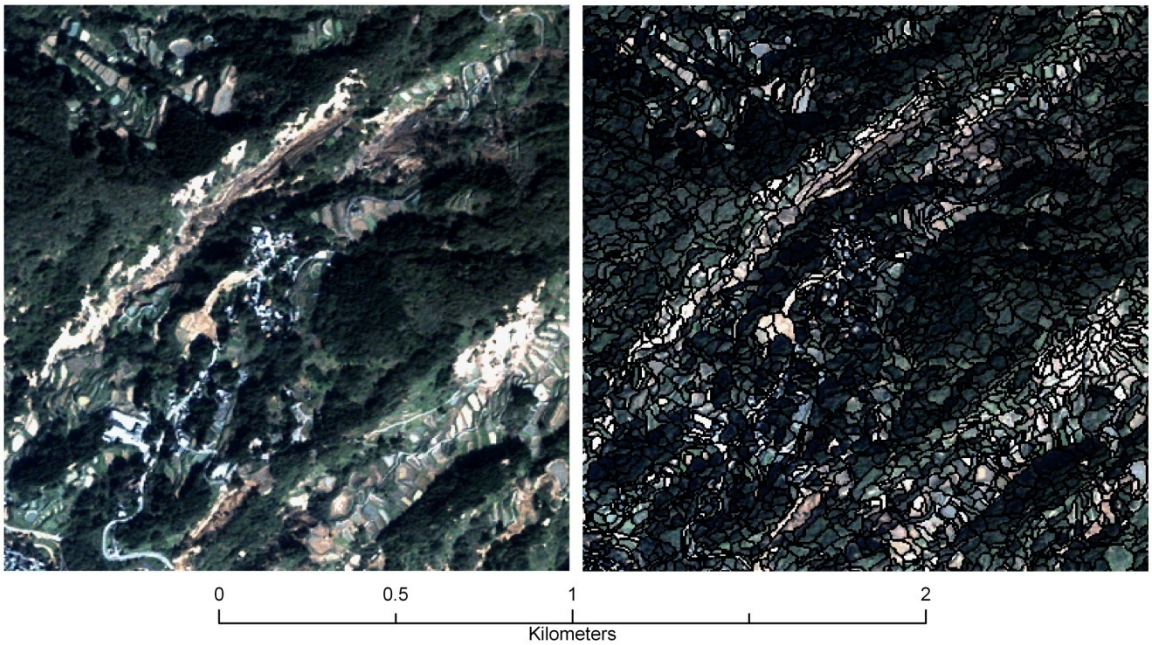

Figure 11. IKONOS imagery, before segmentation (left) and after segmentation (right)

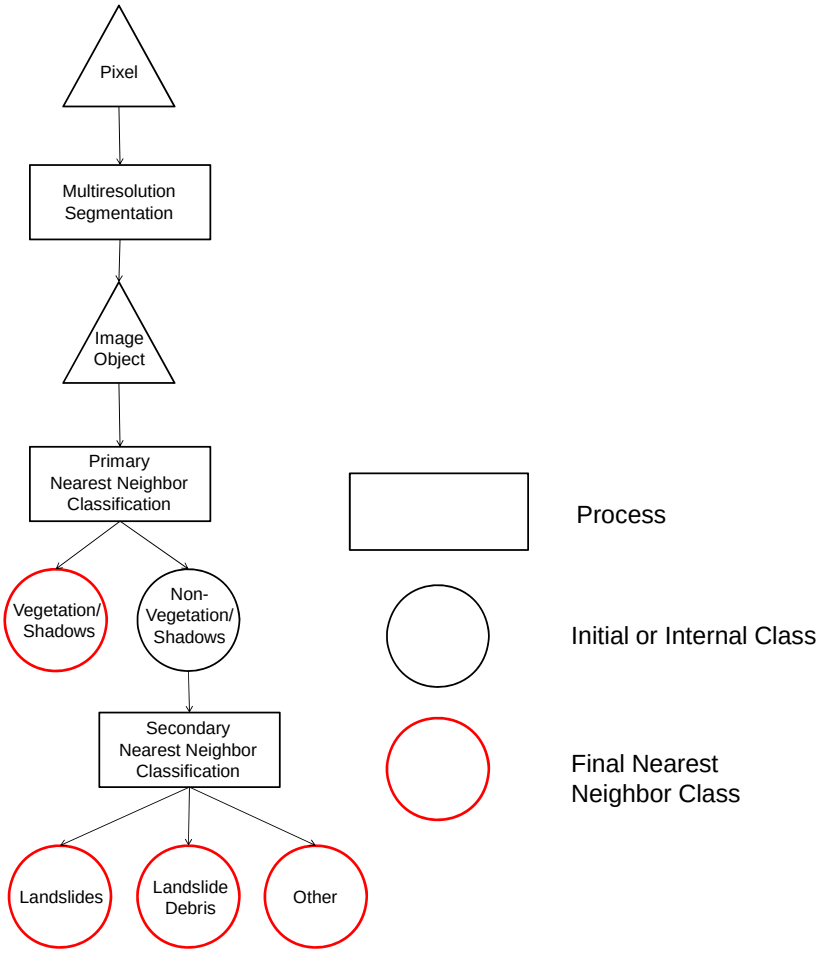

Figure 12. Nearest-neighbor classification flowchart

The primary classification was performed by selecting samples for each class, with care taken to select samples near histogram edges to accurately define the feature space. The secondary classification was performed only on objects previously classified as non-vegetation/shadows. This secondary classification focused on identifying the landslides, landslide debris, and "other" classes. Again, the classification was performed using a feature space containing the mean object value of the IKONOS multispectral data. Unlike the initial classification, an iterative sample selection approach was performed to produce the highest quality classification. Initially, classification was performed using only about five samples per class. The classification was examined, and several incorrectly classified objects were selected as samples for their correct class, and a classification was again performed using the updated training samples. The procedure was repeated until a high-quality classification was produced. Ultimately, 41 samples were selected for the vegetation/shadows class, 53 for the non-vegetation shadows class, 38 for the landslides class, 24 for the landslide debris class, and 162 for the "other" class.

One of the main advantages of the object-oriented classification method is the ability to utilize GIS-like post-classification rules to increase the accuracy of a classified image. The goal of post-classification rules is to emulate the process that the human brain uses to discriminate between different land cover types. For example, the human brain can distinguish a rice paddy from landslide debris because the rice paddy typically exhibits somewhat of an oval shape, and is often surrounded by other rice paddies, while an area of landslide debris generally is close to a landslide, has an irregular shape, and is often surrounded by vegetation. Rules can be implemented to improve the classification accuracy using quantified versions of such observations. The following five rules were used to increase the accuracy of the classification.

Rule 1: *All landslide objects occurring at a distance of greater than or equal to 40 m from the nearest vegetation/shadow object are re-classified as "other".* This rule is implemented to remove confusion related to muddy water in large expanses of agricultural areas that is incorrectly classified as landslides. Because the vast majority of landslides occur very close to or adjacent to vegetated areas, this rule removes the incorrectly classified objects.

Rule 2: *All landslide debris objects with a relative border to vegetation/shadow of greater than 50% are re-classified as landslides.* This rule was applied to include darker appearing landslides as part of the landslides class, rather than the landslide debris class. While eventually the landslide and landslide debris classes will be combined to compute landslide density, subsequent rules (e.g. Rule 4) will attempt to identify landslide debris based on their proximity to landslide objects. The success of these subsequent rules requires application of Rule 2 such that the majority of the landslide area is classified in the landslides class. The relative border refers to the percentage of the total border length of an object which borders objects of another particular class. As most landslides are surrounded by vegetation, this rule re-classifies darker landslides as landslides rather than landslide debris. Generally, the rule did not inadvertently re-classify agricultural areas as landslides because agricultural areas are typically surrounded by little or no vegetation.

Rule 3: *All landslide debris objects adjacent to landslides are re-classified as landslides.* Because the landslide debris class represents a different spectral response than the

landslides class, this rule re-classifies landslide debris objects as landslides if they are directly adjacent to a landslide object.

Rule 4: *All "other" objects with a relative border to landslide objects greater than or equal to 20% are re-classified as landslides.* Because some omission errors in the landslide debris class exist (i.e. landslide debris objects are classified as "other"), this rule seeks to include these objects in the landslides class. This rule re-classifies all "other" objects as landslides if they share 20% or more of their border with landslides. Rule 4 significantly increases the landslide area, because many of the objects classified as "other" which border landslides are now classified as landslides.

Rule 5: *All landslide debris objects occurring more than 120 m from the nearest landside object are re-classified as "other".* This rule seeks to remove commission errors within the landslide debris class, because agricultural areas are often incorrectly classified as landslide debris. Because landslide debris is generally very close to an area classified as landslides, this rule was selected to remove incorrectly classified objects occurring at distances of 120 m or more from a landslide object.

Accuracy Assessment

The accuracy of the object-oriented classification was assessed using site-specific, non-site specific, and qualitative accuracy assessments, following nearly the same procedure as the accuracy assessments utilized for the pixel based classifications. However, because only four final classes were used instead of eight, slight differences exist in the computation of the site-specific and non-site specific accuracies.

Site-specific accuracy was computed using the same ground truth data as the pixel-based classifications. However, the simpler class hierarchy necessitated the combination of several of the ground truth classes. The separate vegetation and shadows classes were combined into a single vegetation/shadows class. The agricultural, muddy water, water, and urban classes were combined to create the "other" class. The landslides and landslide debris classes were not altered. As a result, roughly 2,000 pixels of ground truth were available for the vegetation and shadows classes, 4,000 pixels were available for the "other" class, and 1,000 pixels each were available for the landslides and landslide debris classes.

The confusion matrix for the object-oriented classification (Table 5) shows an overall accuracy of 78.9% and a kappa coefficient of 0.68. The landslides class exhibits remarkably low confusion, with 94% of the ground truth pixels correctly classified. Confusion is highest within the landslide debris class, principally between the landslides class and the "other" class, with 44.7% of the ground truth pixels of the landslide debris class being classified as landslides and 39.0% being classified as "other". Omission errors were very high within the landslide debris class, with 89.8% of the landslide debris ground truth pixels being classified as another class. Both the landslides and landslide debris classes exhibited similar commission errors, of 52%. However, these poor values are not truly representative of the actual accuracy, as many areas which spectrally resemble the landslide debris class were included in the landslides class due to rule implementation. The true accuracy to a user in the field is significantly higher, as landslides and landslide debris represent the same type of land cover, and discrimination between the two classes is not important for the production of a useful classification.

Table 5. Four class confusion matrix, object-oriented classification

Classification	Ground Truth: *Landslides*	*Landslide Debris*	*Other*	*Vegetation and Shadows*	*Commission Error*	*Omission Error*
Landslides	93.6	44.7	14.0	0.0	52.0	6.4
Landslide Debris	0.0	10.2	2.8	0.0	52.1	89.8
Other	6.0	39.0	82.1	0.0	12.1	17.9
Veg. & Shadows	0.4	6.1	1.1	100	5.2	0.0
Total Accuracy	78.9	*Kappa Coefficient*			0.68	

To more accurately assess landslide identification, a confusion matrix was generated that combines the landslides and landslide debris classes in both the classification and ground truth data for a site specific accuracy assessment (Table 6). In this case, the overall accuracy increases to 84.6%, due to the reduction in errors between the landslides and landslide debris classes. However, the landslide and landslide debris classes were left separate in the interest of the final user of the classification. Objects classified as landslides have a much higher probability of actually being landslides than the objects classified as landslide debris because they may be agricultural areas that were not removed through implementation of the post-classification rules. The combination of the classes increases the total errors within the landslide class, with only 74.2% of the ground truth pixels of the combined landslide and landslide debris class correctly classified, compared to 93.6% of the landslide only ground truth pixels being correctly classified as landslides when the classes are left separate.

Table 6. Three-class confusion matrix, object-oriented classification

Classification	Ground Truth: *Landslides*	*Vegetation/ Shadows*	*Other*	*Commission Error*	*Omission Error*
Landslides	74.2	0.0	16.8	31.1	25.8
Veg. & Shadows	3.2	100	1.1	5.2	0.0
Other	22.6	0.0	82.1	12.1	17.9
Total Accuracy	85.6	*Kappa Coefficient*		0.76	

A *non-site specific accuracy* assessment in the form of a landslide density comparison between the object-oriented classification and the GSI landslide map was performed (Figure 13). The landslide and landslide debris classes were combined when computing landslide density. Approximately 74.1% of the blocks exhibited classified landslide densities within +/- 5 percentage points of the landslide map. For mapped landslide densities less than approximately

13%, the classified and mapped landslide densities agree well. For mapped landslide densities above approximately 13%, the classification tends to underestimate landslide area considerably.

A *qualitative accuracy* assessment of the object-oriented classification was performed by visually examining and comparing the classification to the true-color IKONOS multispectral imagery. Overall, it was found that the object-oriented classification identified landslides well, with relatively few classification errors. Figure 14 shows a portion of the classified and the true-color imagery for the same spatial area. The classification identifies nearly every landslide visible in the imagery, with only minor amounts of confusion between the landslides class and other types of land cover. Additionally, most of the landslides are identified in their entirety rather than as a combination of landslides and landslide debris.

Examination of the entire classified image shows that the object-oriented classification accurately identifies medium to large-sized landslides appearing as brightly-colored areas of stripped vegetation. However, smaller landslides, covering approximately 1500 m^2 or less, are sometimes omitted from the classification. This occurs because small landslides are typically below the heterogeneity threshold used in the formation of image objects, and therefore were lumped into image objects consisting of other land cover types, such as vegetation and shadows. Further examination of the classification reveals some confusion between the landslides class and muddy water, generally consisting of commission errors within the landslides class. Several errors were also observed where roads were incorrectly classified as landslides. Commission errors within the landslide debris class resulting from confusion with agricultural areas are notably absent from the classification, mainly due to the post-classification rules that were implemented to improve the overall classification accuracy.

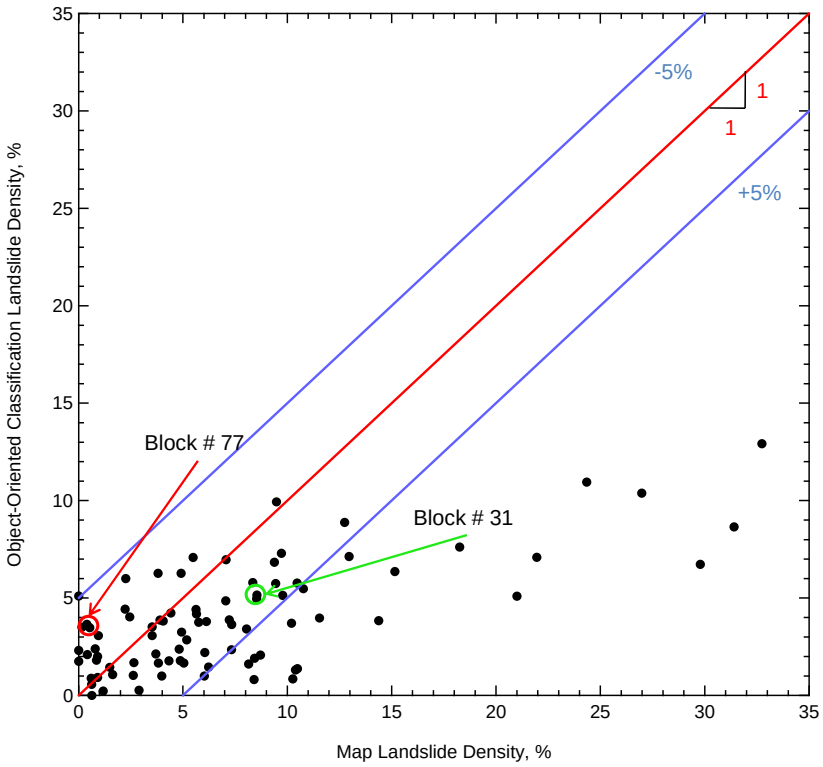

Figure 13. Landslide density for the object-oriented classification,

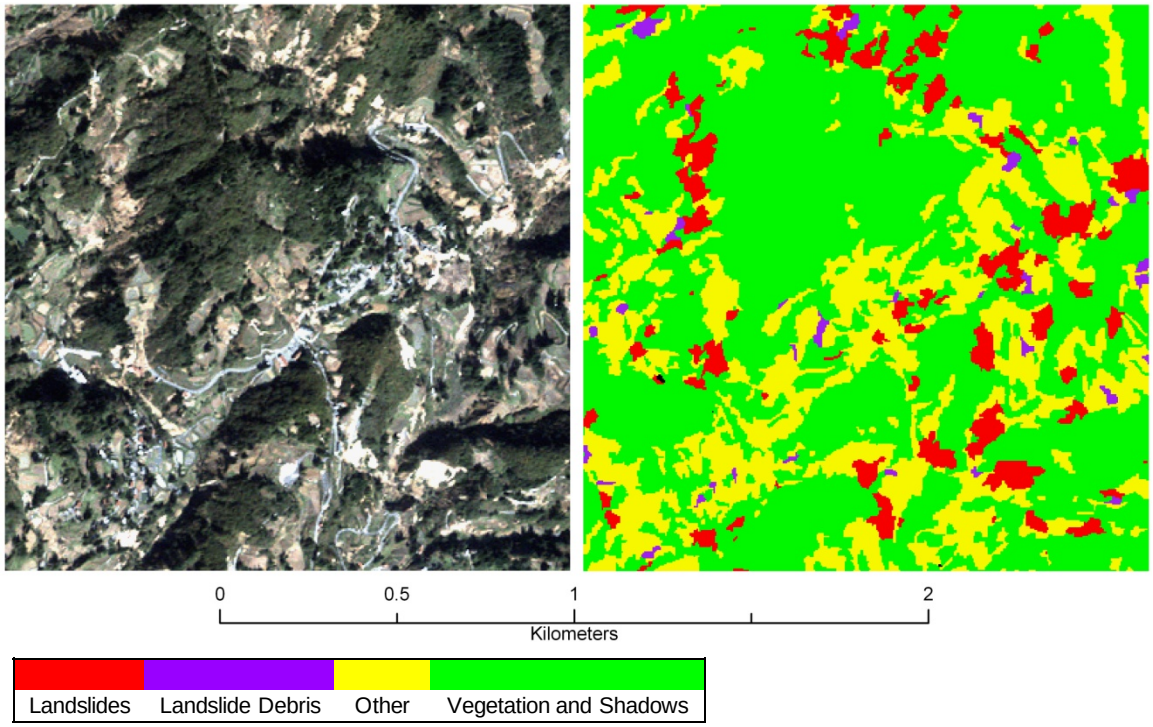

Figure 14. Object-oriented classification (right) and multispectral imagery (left)

COMPARISON OF PIXEL-BASED AND OBJECT-BASED CLASSIFICATIONS

To compare the object-oriented classification and the pixel-based classification methods, a system was developed to rate the qualitative accuracy of each classification as compared to visual interpretation of the multispectral imagery and the GSI landslide map.

The same 1-km^2 blocks used for the non-site-specific accuracy assessments were used for this qualitative comparison between methods. However, the original eight-class hierarchy from the pixel-based classifications was revised to a four-class hierarchy by combining the urban, muddy water, agricultural, and water classes into an "other" class. Combining classes was required so that all classification methods would employ the same four-class hierarchy as the object-oriented classification. Each 1-km^2 block was examined relative to both the original true-color multispectral imagery and the GSI landslide map, and was rated on its qualitative classification accuracy using a five-bin scale, including Very Good, Good, Fair, Poor, and Very Poor. Additionally, the classification method that produced the best relative classification for each block was identified.

Figure 15 displays the classification that was identified as producing the best classification of each block. The object-oriented classification consistently produced the best classification for the individual blocks, with 64.7% of the blocks best-classified by the object-oriented method. 21.7% of the blocks were best-classified by the BHC classification, 7.1% were best-classified by the BPC classification, and only 1.2% were best-classified by the MLC classification. These results agree well with the preliminary qualitative accuracy assessments for each of the classification methods, although they disagree with the more quantitative accuracy assessments (e.g. confusion matrices). The high rating of the object-oriented classification is primarily due to

the lack of large-scale commission errors within the landslide debris class caused by confusion with agricultural areas.

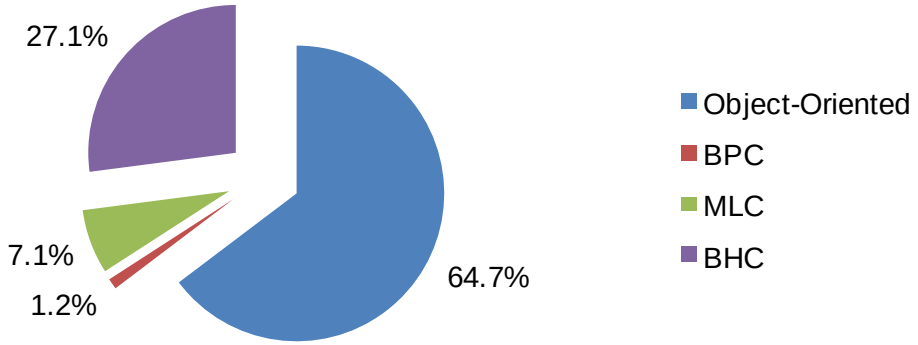

Figure 15. Classification type identified as producing the best classification of each block

A more detailed analysis of the object-oriented classification (Figure 16) shows that 14.1% of the blocks were rated as very good and 43.5% were rated good, resulting in 67.6% of the blocks being rated good or very good. 24.7% were rated fair, and the remaining 17.6% of the blocks were rated as poor or very poor, primarily due to commission errors within both the landslide and landslide debris classes, due to confusion with muddy water and agricultural areas, respectively.

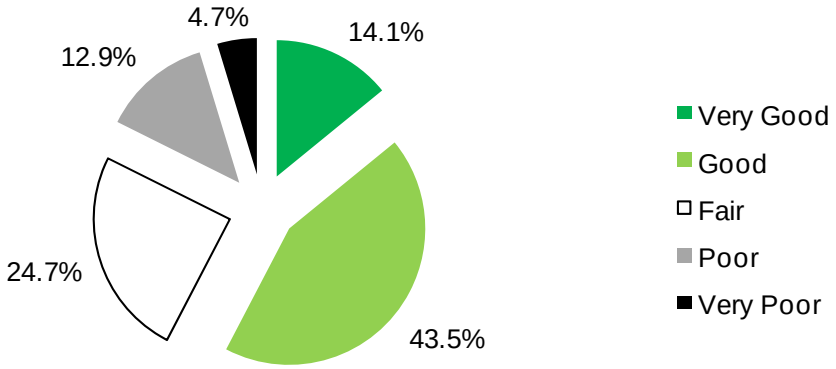

Figure 16. Ratings of blocks classified using the object-oriented method

The rating of the classification produced using the BHC method indicated that only 12.9% of the blocks were classified as very good and another 24.7% were classified as good, leading to 36.6% of the blocks being classified as good or very good. The percentage of blocks classified as good or very good drops by nearly half, from 67.6% to 36.6%, as compared to the object-oriented analysis. 37.5% of the blocks were classified as fair and the remaining 25.9% of the blocks were classified as either poor or very poor. This indicates that the BHC method produces a lower quality classification than the object-oriented method.

The ratings of blocks classified using the BPC method indicates that only 2.4% of the blocks were classified as very good and another 20% were classified as good, leading to 22.4% of the blocks being classified as good or very good. 35.3% of the blocks were classified as fair and the remaining 42.4% of the blocks were classified as poor or very poor. This result indicates that the

BPC method produces a lower quality classification than either the object-oriented or BPC classifications.

The ratings of the blocks classified by the MLC method indicated that only 3.5% of the blocks were rated very good and 18.8% of the blocks were rated good, leading to 22.3% of the blocks being rated good or very good. 35.3% of the blocks were rated fair and the remaining 42.3% of the blocks are rated poor or very poor. This result indicates that the MLC method produces a lower quality classification than the object-oriented, BHC, and BPC methods.

Figure 17 shows all classification methods over the same spatial area, along with the multispectral imagery and interpreted GSI landslide map. Immediately obvious is the very large prevalence of commission errors in the landslide debris class with the MLC method. The BPC method produces a similar classification as the MLC, but with fewer commission errors. Out of the pixel-based methods, the BHC has the lowest prevalence of commission errors within the landslide debris class, yet it tends to correctly classify only portions of landslides. The object-oriented classification has few commission errors within the landslide debris class compared to the other methods, and also identifies most landslides in their entirety. There are, however, some commission errors within the landslides class, due to confusion with muddy water.

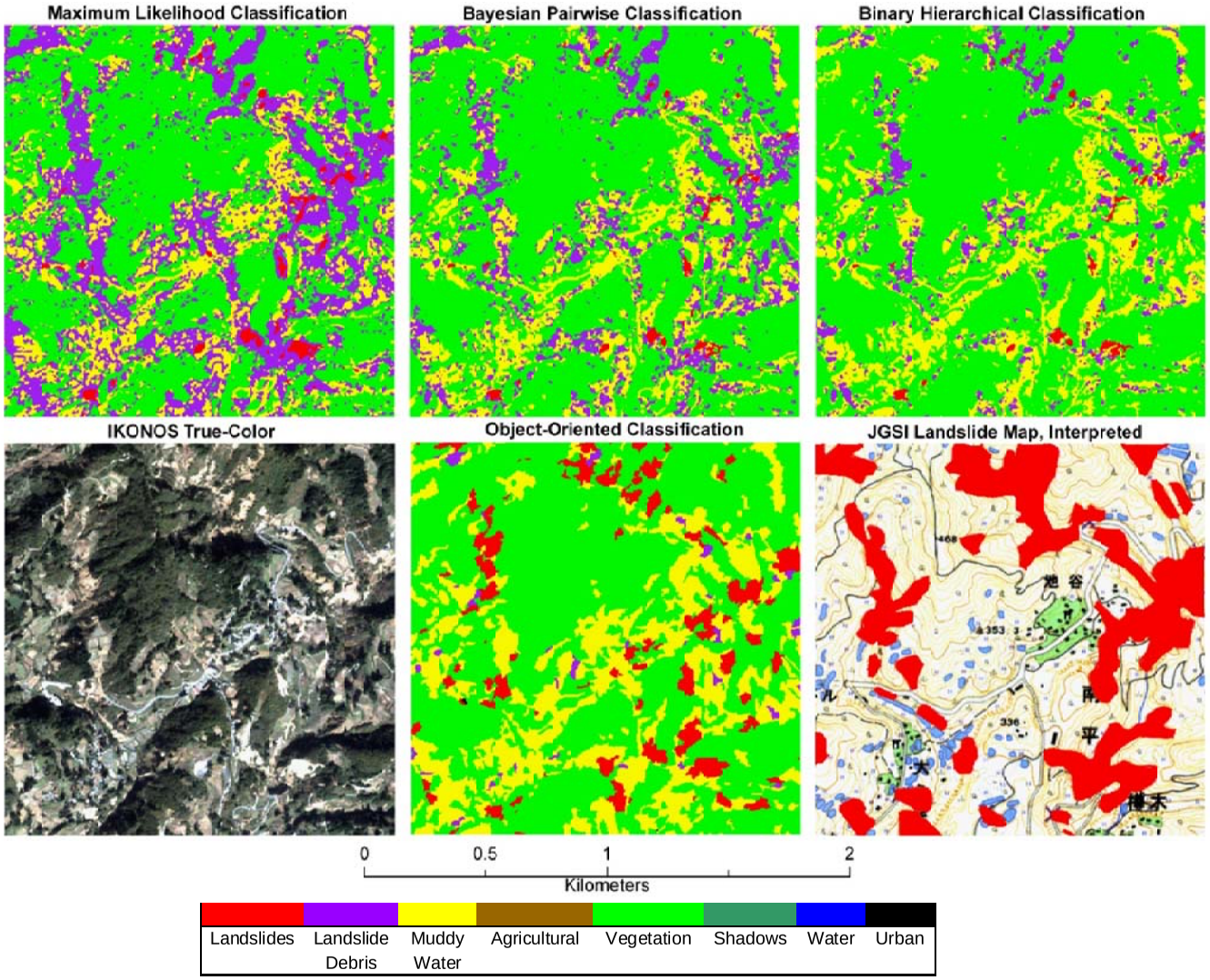
Maximum Likelihood Classification
Bayesian Pairwise Classification
Binary Hierarchical Classification
IKONOS True-Color
Object-Oriented Classification
JGSI Landslide Map, Interpreted
0
0.5
1
2
Kilometers
Landslides
Landslide Debris
Muddy Water
Agricultural
Vegetation
Shadows
Water
Urban

gery,

CHANGE DETECTION OF LANDSAT IMAGERY

Change Detection Analysis

Data collected from the LANDSAT 7 ETM+ sensor was used to perform a change detection analysis over the area affected by the Niigata-Ken Chuetsu earthquake in an effort to identify the earthquake-induced landslides. Pre- and post-event data were collected on July 5, 2004 and November 10, 2004, respectively. These dates were selected because data acquired on dates closer to the earthquake were badly cloud covered. The area affected by the earthquake is included within a single LANDSAT scene, and the imagery exhibited no cloud cover over the area of interest in the pre-event data and very little could cover in the post-event data.

Band selection for change detection analysis focused on determining which spectral band best identified changes in reflectance caused by the removal of vegetation and the exposure of bare soil and rock. To determine which band best identifies landslides, red-green-blue change detection images (i.e. pre-event imagery loaded as blue and green bands and post-event imagery loaded as the red band) were produced using the visible light, NIR, and MIR bands (Figure 18). Increases in the band reflectance will appear red, decreases will appear blue-green, and no change will appear in gray scale. Examination of the resulting images shows that the red band best identifies landslides from the surrounding land covers (Figure 18c). The green and blue bands both work reasonably well for landslide identification (Figures 18a and b), but the changes in reflectance caused by the removal of vegetation appear larger when the red band is used relative to the other visible light bands (Figure 18c). Landslides are either faintly or not observable using the NIR and MIR bands (Figure 18d and e), most likely due to changes in reflectance caused by seasonal changes in vegetation. This effect can be seen between the pre- and post-event true-color imagery (Figure 18f and g), as vegetation appears much greener in the pre-event imagery. As a result, the red band was selected for the change detection analysis.

Reflectance conversion was performed on both pre- and post-event imagery to utilize the data in its most robust format. Histogram matching was also performed by matching the post-event imagery to the pre-event imagery. Histogram matching was performed so each image would exhibit similar brightness distributions, causing landslides to exhibit the largest possible changes in reflectance relative to other land covers. Figure 19 shows red-green-blue change detection images produced using both original and histogram matched imagery. In Figure 19, the landslides stand out from the surrounding terrain far better when histogram matching is performed.

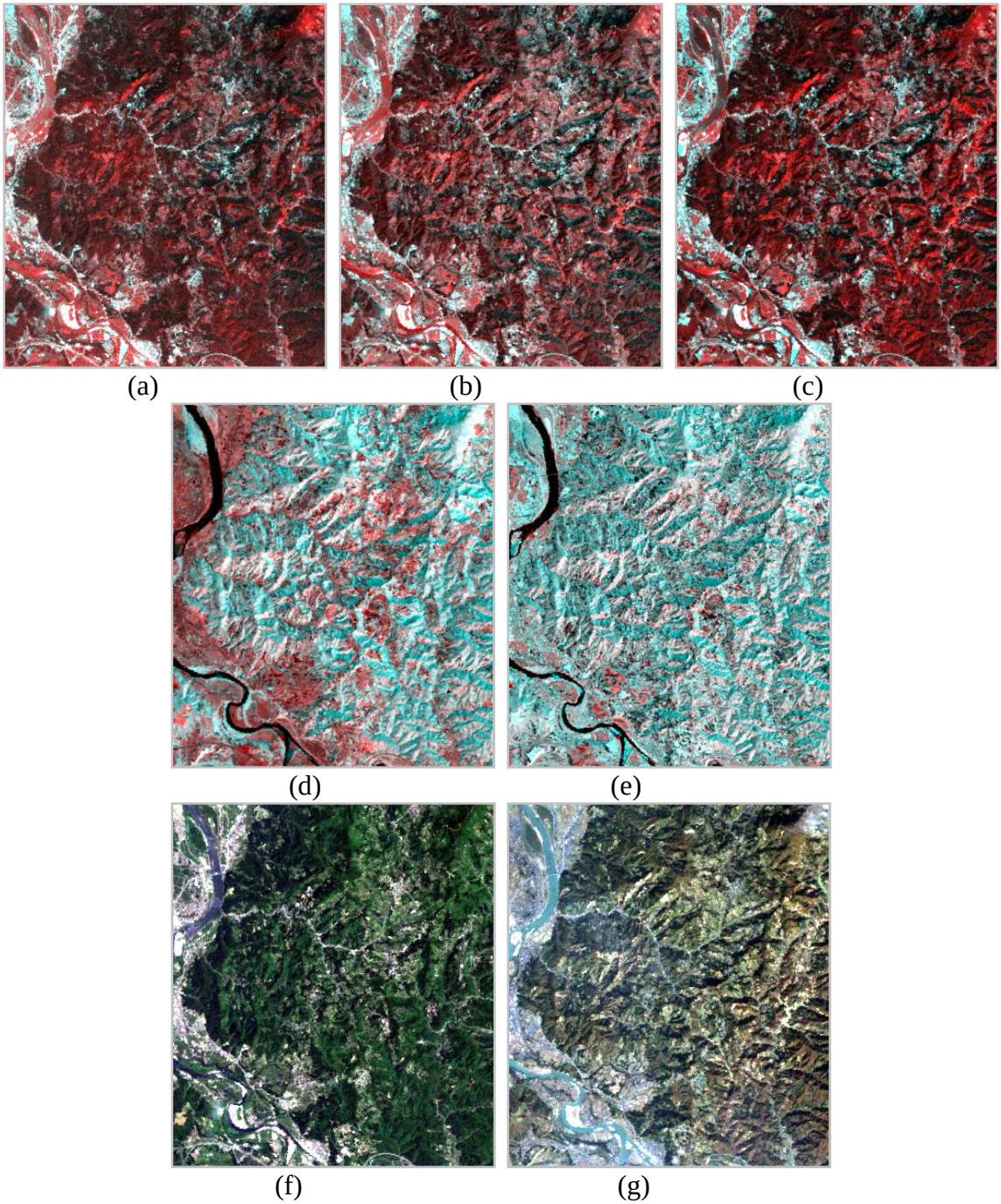

Figure 18. RGB change detection images derived from (a) blue, (b) green, (c) red, (d) NIR, and (e) MIR data. (f) Pre-event and (g) post-event true color multispectral imagery. Scene size is 9.6 km by 10.9 km

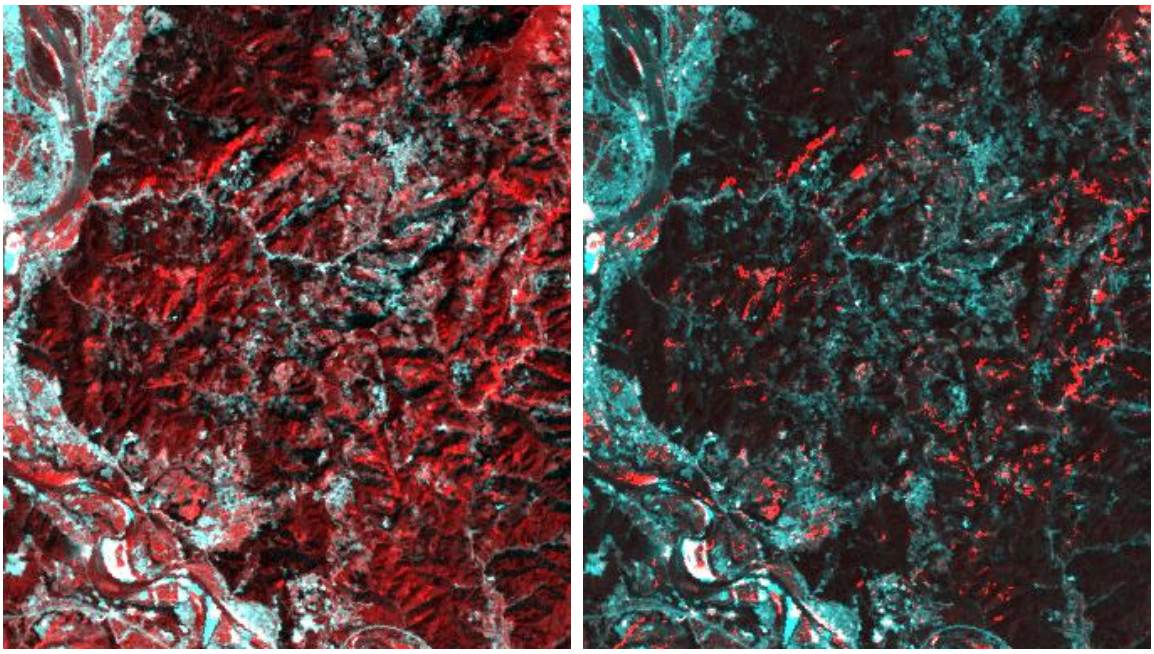

(a) (b)

Figure 19. Red-green-blue change detection images produced on the red band, using (a) original and (b) post-to-pre-event histogram matched data. Scene size is 9.6 km by 10.9 km.

The red-green-blue change detection images indicated that changes in reflectance in the flat-lying alluvial areas near the two large rivers in the area were sometimes similar to landslides (note red areas close to rivers in Figure 19b). Because landslides cannot occur in these flat areas, these areas were masked from the final change detection analysis. A difference map (Post minus Pre) was produced at intervals of reflectance changes of 0.02 (e.g. 0.00 to +0.02, +0.02 to +0.04, etc.) from the post- and pre-event imagery. Figure 20 shows areas defined as landslides using change detection thresholds of >+0.10, >+0.14, and >+0.18, overlain on the post-event multispectral imagery. The change detection threshold of >+0.10 tends to overestimate landslide area when compared with observations from the pre- and post-event multispectral imagery, while the threshold of >+0.18 tends to underestimate landslide area. A change detection threshold of >+0.14 change in reflectance was selected to identify landslides, as it accurately identified most landslides while minimizing commission errors between landslides and other types of land cover.

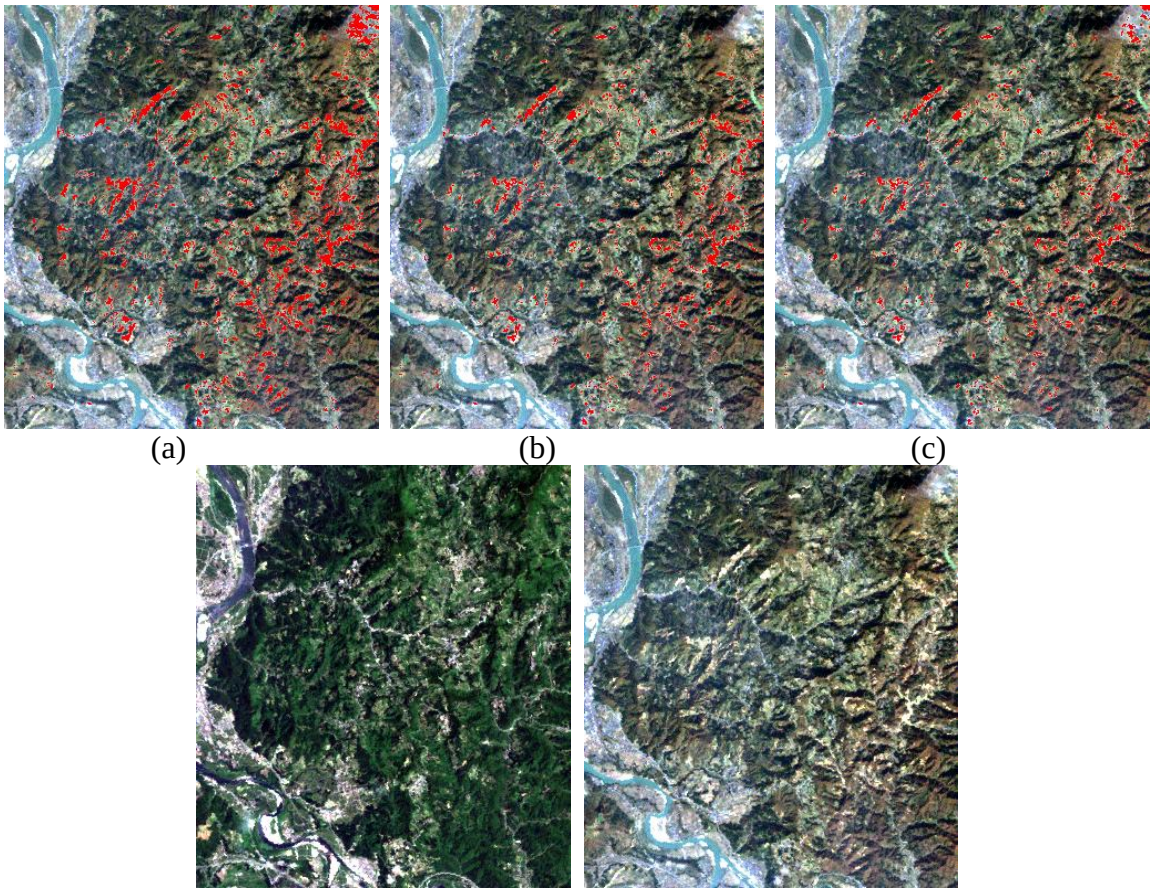

Figure 20. Change detection thresholds of (a) >+0.10, (b) >+0.14, and (c) >+0.18, overlain on post-event multispectral imagery. (d) Pre-event and (e) post-event true color multispectral imagery. Scene size is 9.6 km by 10.9 km.

Accuracy Assessments

The effectiveness of the change detection analysis was evaluated by performing a non-site-specific accuracy assessment utilizing ground truth data in the form of the GSI landslide map. The qualitative accuracy was evaluated through visually inspecting the landslides identified by the analysis relative to the multispectral imagery.

The *non-site-specific accuracy* of the landslide map produced by the change detection analysis was evaluated by comparing the total landslide area obtained from the analysis to that obtained from the GSI landslide map. The change detection analysis identified 2.66 km^2 of landslide area, compared to 6.30 km^2 identified by the GSI landslide map. The identified landslides from these two datasets are shown in Figure 21. Overall, the change detection analysis tends to produce landslide distributions similar to that shown in the GSI landslide map, although the GSI landslide map identifies over twice the landslide area as the change detection analysis. Examination of Figure 21 shows that the differences are primarily due to the differences in the size of landslides shown in each method, rather than the lack of identification of landslides in the change detection analysis. The landslides appear much larger in the GSI landslide map than in the multispectral imagery, typically due to large portions of the mapped landslides being covered with displaced vegetation, which leads to no change in reflectance

relative to the land cover before the earthquake occurred. Despite the large difference in total landslide area, the landslide map derived from the LANDSAT data shows a consistent trend of landslide distribution relative to the JGSI map. Specifically, the larger density of landslides in the eastern section of the imagery is identified.

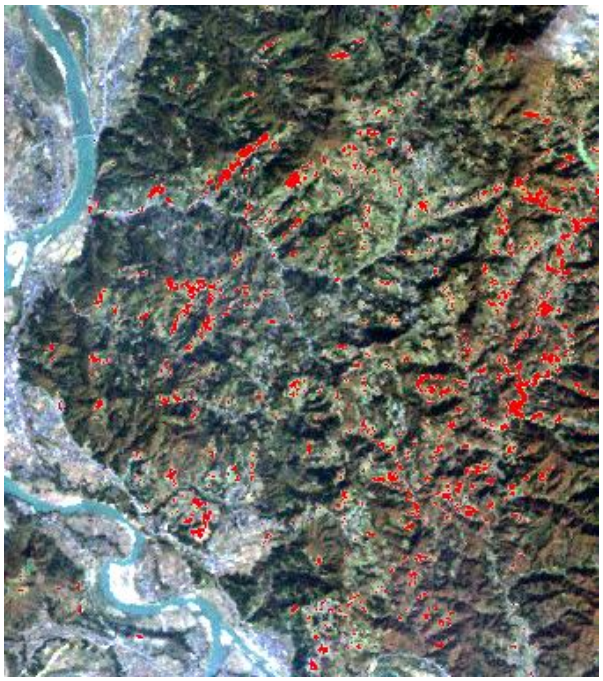

(a)

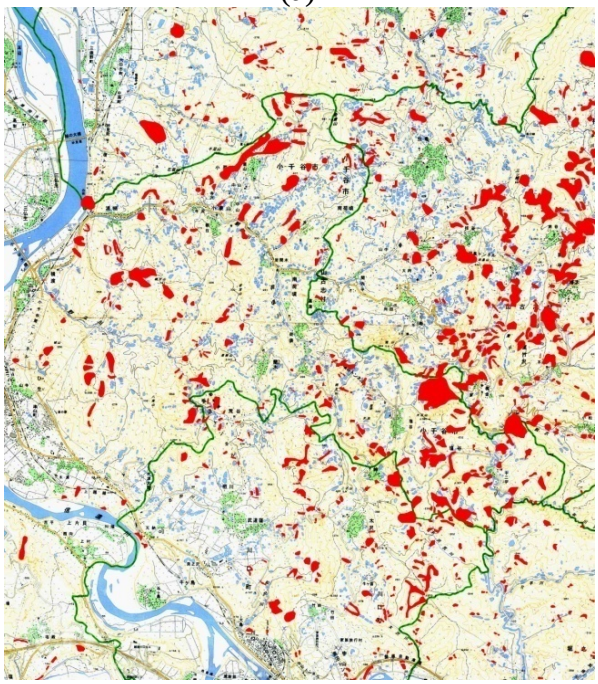

(b)

Figure 21. Landslide distributions from (a) LANDSAT change detection analysis and (b) GSI landslide map. Landslides overlain in red. Scene size is 9.6 km by 10.9 km.

Qualitative accuracy assessment via examination of the landslide distribution from the change detection analysis overlain on the post-event imagery (Figure 22) reveals that the change detection analysis accurately identifies landslides which stripped away vegetation from hillsides across the imagery. No landslides visible in the imagery appear to be omitted from the change detection analysis; however the coarse resolution of the data and relatively small spatial areas of landslides makes visual identification of smaller landslides in the imagery somewhat difficult.

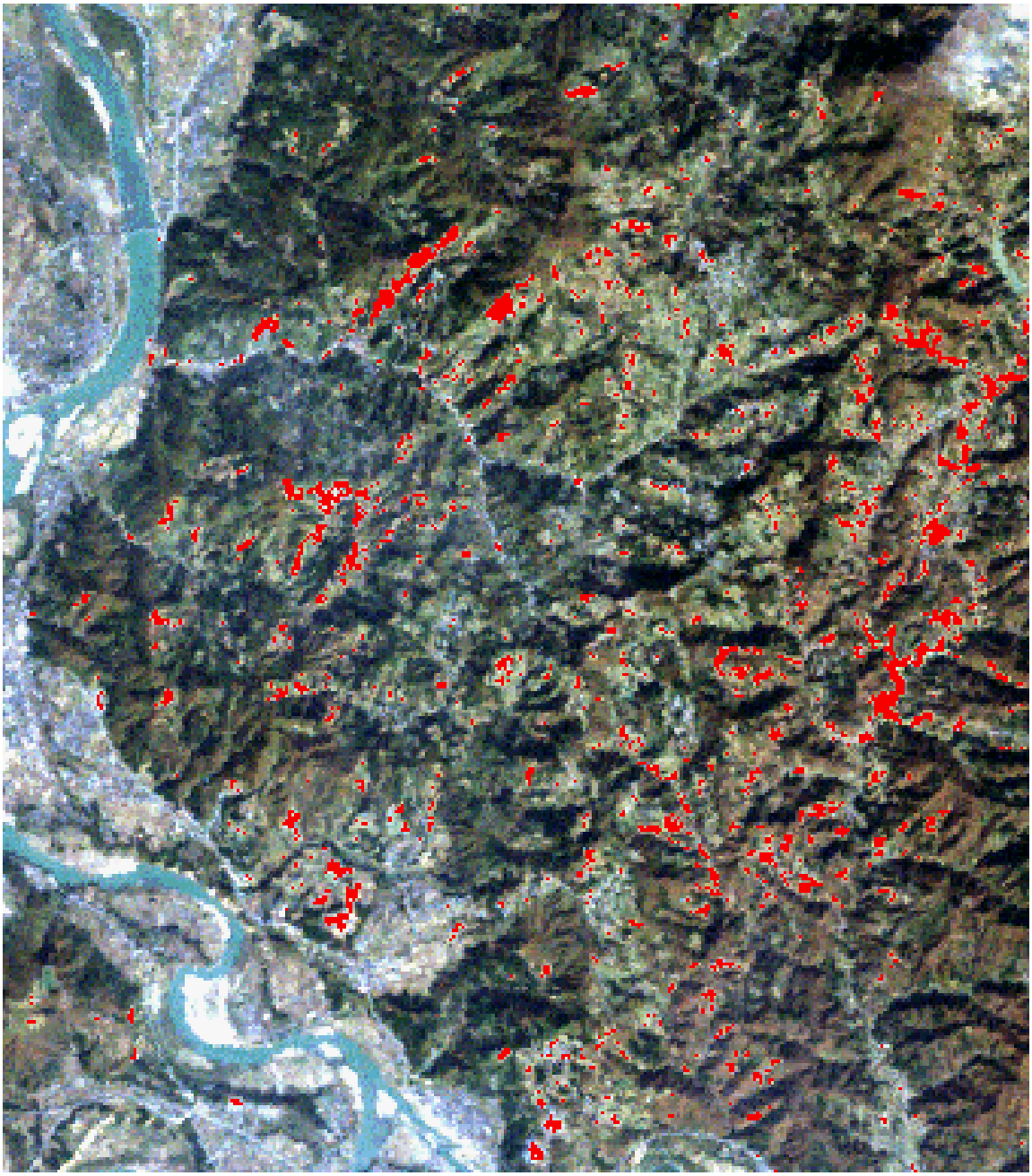

Figure 22. Post-event LANDSAT true-color imagery with landslides obtained from change detection analysis overlain in red. Scene size is 9.6 km by 10.9 km.

CONCLUSIONS

This report presents the methodology, results, and assessment of the use of remotely sensed imagery for mapping landslides caused by the 2004 Niigata-Ken Chuetsu, Japan earthquake. The main goals of this research were to explore the use of semi-automated techniques to produce post-disaster damage maps showing the locations of landslides caused by earthquakes. Visual interpretation of post-event imagery, semi-automated classification of post-event imagery, and change detection analyses between pre- and post-event imagery were explored for their relative ease of use and accuracy.

Post-event high-resolution imagery for the Niigata-Ken Chuetsu earthquake from the IKONOS satellite sensor was classified using pixel-based (MLC, BPC, and BHC) and object-oriented classification techniques. Out of the pixel-based classification methods, the BHC produced the highest-quality classification. Both the BPC and MLC methods exhibited substantial amounts of confusion between agricultural areas and the landslide debris class, with the BPC method exhibiting slightly less confusion. The BHC method, however, produced far fewer commission errors within the landslide debris class, which is the principal reason for its selection as the best pixel-based classifier used in this research. The object-based classification produced a superior assessment of the landslide distribution relative to the pixel-based methods. The improved identification of landslides is mainly due to the application of post-classification rules that move incorrectly classified objects to their correct class based on their relationship to the classification of other objects.

Landslide density comparisons between the classified post-event imagery and the GSI landslide map showed that all classification methods substantially underestimated landslide densities, particularly at larger landslide densities (i.e., greater than 10 to 15%). However, these large differences in the mapped and classified landslide densities were caused by the fact that many of the landslides were covered by some or significant vegetation. Due to this discrepancy, the landslide density derived from classification methods should only be considered a preliminary assessment of the landslide density. Manual interpretation of the full landslide extents should follow the semi-automated assessments.

Although the semi-automated classification methods were able to provide decent estimates of landslide distributions, they have many shortfalls. The amount of time required to define a class hierarchy, perform classifications of the imagery, and troubleshoot the classifications was found to be far greater than the amount of time required to manually interpret the imagery. Additionally, manual interpretation is often more accurate than semi-automated classification.

Change detection analysis was performed using pre- and post-event imagery from the LANDSAT satellite (28.5 m spatial resolution) for the Niigata-Ken Chuetsu earthquake. The low spatial resolution of the LANDSAT data allowed landslides to be mapped over large areas in a short amount of time. Change detection analyses are fundamentally simple to perform in that accurate class hierarchies and classification schemes do not need to be developed. Rather, change detection analysis only involves data pre-processing and the determination of a change detection threshold. The spatial distribution of landslides produced by the change detection analysis is similar to that found in the GSI map, indicating that the change detection analysis was generally effective for determining broad landslide distributions in this area. However, the total area of landslides was underestimated relative to the GSI map.

For imagery analysis of future earthquakes exhibiting a large amount of earthquake-induced landslides, it is recommended that low to medium resolution data, such as LANDSAT, be used

for quick, large-scale landslide mapping. Manually interpreted high-resolution data can be used for mapping smaller areas in greater detail. Semi-automated post-event classification is often too time consuming to be of use for landslide mapping, as manual interpretation can be performed far quicker and more accurately.

REFERENCES

Campbell, James B. 2007. *Introduction to Remote Sensing*. New York: The Guilford Press

Crawford, M.M., S. Kumar, M.R. Ricard, J.C. Gibeaut, and A. Neuenschwander 1999. "Fusion of Airborne Polarimetric and Interfermetric SAR Data for Classification of Coastal Environments," *IEEE Trans. Geoscience and Remote Sensing*, vol. 37, 1306-1315.

Geographical Survey Institute of Japan. 2004. "Disaster Map – October 23, 2004 Niigata-Ken Chuetsu Earthquake at 1:30,000 scale". (2004. In Japanese)

Keefer, David K. 2002. "Investigating Landslides Caused by Earthquakes – A Historical Review." *Surveys in Geophysics* 23: 473-510.

Kieffer, D.S., Jibson, R., Rathje, E.M., and Kelson, K. 2006. "Landslides triggered by the 2004 Niigata Ken Chuetsu, Japan, Earthquake" *Earthquake Spectra* 22 (S1): S47-S73.

Kumar, S., Crawford, M.M., and Ghosh, J., 1999 "A Versatile Framework for Labeling Imagery with a Large Number of Classes," *Proceedings of the International Joint Conference on Neural Networks* Washington, D.C., July 10-16.

Kumar, S., Ghosh, J., and Crawford, M.M., 2002. "Hierarchical Fusion of Multiple Classifiers for Hyperspectral Data Analysis," *International J. Pattern Analysis and Applications* vol. 5, no.2, pp. 210-220.

Rathje, E.M., Kayen, R., and Woo, K.S. 2006 "Remote Sensing Observations of Landslides and Ground Deformation from the 2004 Niigata Ken Chuetsu Earthquake." *Soils and Foundations*, Japanese Geotechnical Society 46(6):831-842.

Scawthorn, C. and Rathje, E.M. 2006. "The 2004 Niigata Ken Chuetsu, Japan, Earthquake." *Earthquake Spectra* 22 (S1): S1-S8.

PUBLICATIONS RESULTING FROM THIS WORK (TO DATE)

Carr, Lucas (2009) *The Application of Remote Sensing for Mapping Earthquake-Induced Landslides from the 2008 Wenchuan, China and 2004 Niigata-Ken Chuetsu, Japan Earthquakes*, M.S. Thesis, University of Texas, Austin, TX, 298 pp.